arXiv:hep-ph/0006337v1 29 Jun 2000

Impact of Hadronic Axions on Black Hole Accretion Discs and Neutron Stars

Diplomarbeit
von
Klaus Böcker

München, September 1999

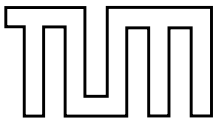

Physik-Department der Technischen Universität München
Institut für Theoretische Physik T30
Prof. Dr. Manfred Lindner
Angefertigt am Max-Planck-Institut für Physik
(Werner-Heisenberg-Institut)
bei Dr. Georg Raffelt

Zusammenfassung

Axionen entstehen bei der Lösung des „starken CP-Problems“ mit Hilfe der Peccei-Quinn-Symmetrie. Der astrophysikalisch und kosmologisch prinzipiell erlaubte Bereich von Axionenmassen beschränkt sich auf zwei Regionen: zum einen „leichte“ Axionen mit Massen zwischen 10^{-5} und 10^{-3} eV, die kalte dunkle Materie (CDM) des Universums darstellen, zum anderen „schwere“ Axionen aus dem sogenannten „hadronischen Axionenfenster“ mit Massen um 10 eV. Ihre Existenz würde mit $\Omega_a \approx 0.1$–0.3 zur heißen dunklen Materie (HDM) beitragen.

Die genaue Breite des hadronischen Axionenfensters hängt stark vom zugrundeliegenden Axionenmodell ab. Deswegen werden in dieser Arbeit zunächst die bestehenden und für hadronische Axionen relevanten astrophysikalischen Argumente neu überprüft. Das Ergebnis ist, dass Axionen mit einer Masse zwischen 10 und 20 eV nicht ausgeschlossen werden können, falls sie keine Baum-Niveau-Kopplungen an gewöhnliche Quarks und Leptonen besitzen und wenn gleichzeitig ihre Kopplung an Photonen extrem stark unterdrückt ist.

Hadronische Axionen wechselwirken in erster Linie mit Protonen und Neutronen. Als Konsequenz können sie in nukleonenreicher Materie durch den Bremsstrahlungsprozess $N + N \to N + N + a$ erzeugt werden. Daher – um das hadronische Axionenfenster genauer zu untersuchen – betrachten wir Akkretionsscheiben um Schwarze Löcher und isolierte Neutronensterne. Erstere können während des Kollaps eines Neutronendoppelsterns entstehen und liefern ein vielversprechendes Modell für kurze Gammastrahlungsausbrüche. Gemäß diesem entstehen in der Akkretionsscheibe Neutrinos und Antineutrinos, von denen sich ein Teil in Elektron-Positron-Paare und weiter in hochenergetische Gammastrahlung umwandelt. Ein zusätzlicher Energieverlust durch die Emission hadronischer Axionen könnte die Luminosität der Gammastrahlungsausbrüche erheblich verringern. Wir stellen fest, dass Axionen mit einer Masse von etwa 11 bis 66 eV einen wichtigen Einfluss auf Gammastrahlungsausbrüche haben, wobei diese quantitativen Aussagen jedoch stark vom zugrundeliegenden Modell der Akkretionsscheibe und dem des Schwarzen Lochs abhängen.

Signifikantere Grenzen für die Masse hadronischer Axionen ergeben sich aus der Betrachtung isolierter Neutronensterne. Mit einem einfachen Modell für das Abkühlungsverhalten eines Neutronensterns zeigen wir, dass die gemessenen Oberflächentemperaturen der Pulsare PSR 1055-52, PSR 0630+178 (Gemina) und PSR 0656+14 zu hoch sind, um mit der Existenz hadronischer Axionen im Einklang zu stehen. Diese Erkenntnis wird durch numerische Berechnungen der Neutronensternkühlung von Umeda et al. [8] bestätigt, deren Ergebnisse wir einer erweiterten Interpretation im Hinblick auf hadronische Axionen unterziehen.

Acknowledgment

I am greatly indebted to my supervisor, Georg Raffelt, for introducing me to this intriguing subject, and for his support and advice.

Furthermore, I have benefited from the friendly and stimulating atmosphere at the Max-Planck-Institut für Physik, München. Thanks to all the students and postdocs, especially to Robert Buras for stimulating discussions, and Maurice Lausberg and Björn Pötter for teaching me to play table tennis.

Last but not least, I would like to thank my partner Katharina Macketanz for putting up with me.

Contents

Chapter 1

Introduction

The axion was proposed in 1977 to solve the CP problem of QCD ("strong CP problem"). Since then, more than 500 research papers about axions and related topics have been published [1]. Evidently, axions have been a stimulating subject! The main reason for this steady interest is that axions not only provide an elegant solution to the strong CP problem, but are also attractive from a cosmological perspective. More specifically, there are two regions of axion masses where these particles could constitute some or all of the cosmic dark matter: Axions with a mass in the range $m_a \approx 10^{-5}$–10^{-3} eV are an ideal candidate for cold dark matter (CDM), and two current experiments actually search for these very light particles [2, 3]. Moreover, it was recently claimed that "heavy" axions in the so-called "hadronic axion window" around 10 eV provide a hot dark matter (HDM) component with $\Omega_a \approx 0.1$–0.3, exactly the amount needed in mixed dark matter scenarios [4].

While there is no doubt that axions in the CDM window are astrophysically and cosmologically allowed [5], the situation is less clear for the HDM range because the existence and exact width of the hadronic axion gap strongly depends on details of the axion model. Therefore, firstly we have re-examined the hadronic axion window and have found that axions without tree-level couplings to ordinary quarks and leptons ("KSVZ-type axions") and masses between 10 and 20 eV are not excluded by previous astrophysical arguments if their coupling to photons $g_{a\gamma\gamma}$ is less than approximately 3×10^{-11} GeV^{-1}. This value is nearly one hundred times smaller than in generic axion models, implying a strong suppression of the photon coupling for these models to be viable in the hadronic mass range. It turns out that one can construct models where this suppression arises as a accidental

cancellation between two independent contributions to the axion-photon coupling [6]. Therefore the hadronic axion window is indeed open. Henceforth, the term "hadronic axions" shall refer to models with severely suppressed photon couplings, i.e. they are a subclass of "KSVZ-type axions," a term which applies to models without tree-level coupling to ordinary quarks and leptons.

Hadronic axions are very weakly interacting particles, and one might think that they can not have any significant influence on astrophysical objects. However, as a consequence of the axion-pion mixing, their effective nucleon coupling is comparable to those of generic axion models. This means that those astrophysical objects which mainly consist of nuclear matter are suitable candidates to explore the hadronic axion window. Therefore, we consider isolated neutron stars and black hole accretion discs (BHADs) as axion laboratories—both types of objects have not been studied in this context.

Accretion discs around black holes are possible outcomes of neutron star mergers and have recently been discussed in connection with a very intriguing class of mysterious astrophysical phenomena: the gamma-ray bursts, short and intense photon eruptions with energies of typically 100 keV–1 MeV. According to the BHAD model, a gamma-ray burst develops when neutrinos, which are produced inside the hot accretion torus, are converted into a photon burst. The crucial point is that the initial neutrino luminosity must be extraordinarily large to account for the observed energies in photons in the range 10^{50}–10^{53} erg. However, numerical neutron star merger simulations [7] yield total neutrino luminosities of about 10^{53} erg s^{-1}, enough to explain short and weak gamma-ray bursts with energies in the ballpark of 10^{50}–10^{51} erg. This situation could change if axions existed in the hadronic axion window. Produced via the bremsstrahlung process $N + N \to N + N + a$, they represent a novel, important energy-loss mechanism in accretion discs. In this case, the neutrino luminosity would be significantly reduced, dimming the observed gamma-ray burst signal. Put another way, the requirement that the axion luminosity must not exceed the neutrino emission puts an upper axion mass limit, which we find in the range 10–100 eV, i.e. hadronic axions could have an impact on the evolution of gamma-ray bursts. However, this bound depends on unknown details of the BHAD model. Nevertheless, although precise and reliable statements about the influence of hadronic axions on gamma-ray bursts require a deeper understanding of these fascinating celestial objects, it is quite certain that hadronic axions if they were found have to be included in present BHAD models.

Finally, we discuss the cooling of neutron stars by means of hadronic axion emission. We set up a simple cooling model and show that recently measured surface temperatures of the isolated neutron stars PSR 1055-52, PSR 0630+178 (Gemina), and PSR 0656+14 are too high to be in accordance with hadronic axion emission because these particles significantly accelerate the energy loss of the star. Furthermore, we review a recent calculation of Umeda et al. [8] who studied neutron star cooling including axions by means of numerical simulations. However, they did not discuss the implications for hadronic axions. It turns out that an interpretation of their results with regard to the hadronic axion window confirms the outcome of our simple model, namely that hadronic axion emission is in conflict with the observed surface temperatures of neutron stars.

Chapter 2

Summary of Axion Physics

By way of introduction, we briefly summarize the most important aspects of axion physics. First, we outline how axions solve the strong CP problem, and how they arise as a simple extension of the Standard Model. Then, the KSVZ axion is discussed in more detail. Finally, the couplings of axions to ordinary matter, i.e. to photons, electrons and nucleons are discussed.

2.1 Motivation for Axions: The Strong CP Problem

In weak interactions one observes CP violation, whereas the strong interactions are known to respect P and CP invariance to very high accuracy. This CP invariance of the strong sector is a problem because QCD predicts CP violation as a consequence of two different mechanisms. First, there is the topologically nontrivial ground state of QCD, the so-called "Θ-vacuum". Second, the axial transformation, necessary to diagonalize the complex quark mass matrix, also leads to CP violation. Both effects together cause an additional nonperturbative term in the QCD Lagrangian,

$$\mathcal{L}_{\rm SM}^{\rm eff} = \mathcal{L}_{\rm SM}^{\rm pert} + \bar{\Theta}\frac{g_s^2}{32\pi^2}\, G_a^{\mu\nu}\, \tilde{G}^a_{\mu\nu}\,, \tag{2.1}$$

where $\mathcal{L}_{\rm SM}^{\rm pert}$ is the perturbative part of the Standard Model Lagrangian, g_s the strong coupling constant, $G_a^{\mu\nu}$ the color field strength tensor, $\tilde{G}^a_{\mu\nu} \equiv \frac{1}{2}\epsilon_{\mu\nu\rho\sigma}\, G^{a\rho\sigma}$ its dual, and $\bar{\Theta} = \Theta + \mathrm{Arg\ det} M$. The ϵ tensor that occurs in the definition of $\tilde{G}$ implies that $\mathcal{L}_{\rm SM}^{\rm eff}$ is not invariant under parity, and thus odd under CP. Note

that the effective CP violating parameter $\bar{\Theta}$ is the sum of a QCD contribution—the vacuum angle Θ—and an electroweak part—Arg det M—related to the phase structure of the quark mass matrix M. The experimental bound on the neutron electric dipole moment requires that

$$|\Theta + \text{Arg det}M| \lesssim 10^{-9}. \tag{2.2}$$

Now, it is difficult to understand why a compound quantity like $\bar{\Theta}$, which is a sum of two very different contributions, should be so small. This fine-tuning problem is known as the strong CP problem.

The strong CP problem can be elegantly explained by introducing an additional global, chiral symmetry with an associated current and charge: the Peccei-Quinn-symmetry $U(1)_{\text{PQ}}$ and the Peccei-Quinn charge [9]. Its existence requires certain enhancements of the Higgs sector of the Standard Model so that its enlarged symmetry group becomes $SU(3)_C \times SU(2)_L \times U(1)_Y \times U(1)_{\text{PQ}}$. However, it should be stressed that $U(1)_{\text{PQ}}$ is a global symmetry and not a gauge symmetry. In typical axion models, PQ symmetry is achieved by introducing additional Higgs fields Φ with degenerate vacua; at least one is necessary. However, in the real world the chiral symmetry $U(1)_{\text{PQ}}$ is not observed, hence it must be spontaneously broken at an energy scale f_a; the associated Nambu-Goldstone boson is the axion. Under a PQ transformation the axion field $a(x)$ shifts as

$$a(x) \to a(x) + \alpha\, f_a\,, \tag{2.3}$$

where α is the parameter associated with the $U(1)_{\text{PQ}}$ transformation. Now we come to the essential feature of the PQ mechanism: the PQ symmetry $U(1)_{\text{PQ}}$ is only exact at the classical level. At the quantum level, however, it is broken by the Adler-Bell-Jackiw anomaly because the PQ symmetry is chiral. As a result, an additional term appears in the effective Lagrangian of equation (2.1),

$$\mathcal{L}^{\text{eff}}_{\text{SM}} = \mathcal{L}^{\text{pert}}_{\text{SM}} + \bar{\Theta}\frac{g_s^2}{32\pi^2}\, G^{\mu\nu}_a\, \tilde{G}^a_{\mu\nu} + \xi\, \frac{a}{f_a}\frac{g^2}{32\pi^2}\, G^{\mu\nu}_a\, \tilde{G}^a_{\mu\nu}\,, \tag{2.4}$$

where ξ is a model dependent parameter. The ξ-term is very similar to the CP violating $\bar{\Theta}$-term and provides an effective potential $V_{\text{eff}}(a)$ for the axion field $a(x)$. This potential implies that the degeneracy of the vacuum is removed. Peccei and Quinn showed that the vacuum expectation value of the axion field, i.e. the value of $a(x)$ where $V_{\text{eff}}(a)$ has its minimum, is given by

$$\langle a(x)\rangle = -\frac{f_a}{\xi}\bar{\Theta}\,. \tag{2.5}$$

Now one introduces a physical axion field $a_{\rm phy}$, which is defined as excitations around the vacuum expectation value (2.5), i.e.

$$a(x)_{\rm phy} \equiv a(x) - \langle a(x) \rangle \,, \tag{2.6}$$

and substitutes it into expression (2.4). In doing this, the $\bar{\Theta} G\tilde{G}$ term is eliminated, and therefore the strong CP problem is solved. Furthermore, one is left with an axion-gluon interaction of the form $a_{\rm phy}\, G\tilde{G}$—obviously an immediate outcome of every axion model. As a result of this generic axion-gluon coupling, axions pick up a small mass of order

$$\begin{aligned} m_a &\approx \frac{m_\pi f_\pi}{f_a} \\ &\approx 6 \text{ eV} \left(\frac{10^6 \text{ GeV}}{f_a} \right), \end{aligned} \tag{2.7}$$

where $f_\pi \approx 93$ MeV is the pion decay constant and $m_\pi = 135$ MeV the pion mass. As the axion has a mass, it is actually a "pseudo Nambu-Goldstone boson."

In summary, we arrive at the following Lagrangian, where from now on a stands for the physical axion field $a_{\rm phy}$,

$$\begin{aligned} \mathcal{L}^{\rm eff}_{\rm SM} &= \mathcal{L}_{\rm SM} + \frac{1}{2} \partial_\mu a \, \partial^\mu a \\ &\quad + \mathcal{L}_{\rm int} \left(\frac{\partial_\mu a}{f_a}, \, \psi \right) + \xi \frac{a}{f_a} \frac{g^2}{32\pi^2} \, G^{\mu\nu}_a \, \tilde{G}^a_{\mu\nu} \,. \end{aligned} \tag{2.8}$$

The second term is the kinetic energy of the axion field, the third represents possible interactions of the axion with fermions ψ and has to be in agreement with the classical invariance under $U(1)_{\rm PQ}$, i.e. under the transformation (2.3). Hence we conclude that the axion field a may enter the interaction Lagrangian $\mathcal{L}_{\rm int}$ only through derivative terms $\partial_\mu a$.

2.2 Axion Models

2.2.1 Standard Axion and Invisible Axions

Let us now look at different axion models which are based on these general ideas. First, we consider the question how the axial symmetry $U(1)_{\rm PQ}$, which solves the strong CP problem, can be reconciled with the Standard Model. In the Standard Model one introduces a complex scalar field, the well-known Higgs field

ϕ. It is an $SU(2)_L$ doublet, i.e. its weak isospin is $I_W = \frac{1}{2}$. Furthermore, its weak hypercharge is $Y = 1$. As a consequence of the Higgs mechanism, all boson and fermion masses are generated by this Higgs field ϕ. The four phases of the isodoublet ϕ provide four additional degrees of freedom. Three of them provide the longitudinal degrees of the $W^{\pm}$ and Z^0, and the remaining phase ends up as the Higgs boson. So, in the Standard Model there is no room for axions. Another way to see this is to recall the transformation properties of the Standard-Model Lagrangian under axial transformations. In particular, consider the Yukawa-coupling terms

$$\mathcal{L}_{\rm Yuk} = -G_d\, \bar{q}_L\, \phi\, d_R - G_u\, \bar{q}_L\, \phi_c\, u_R + \text{h.c.}\ , \tag{2.9}$$

where $\bar{q} = (\bar{u}, \bar{d})$ and $\phi_c \equiv i\tau_2 \phi^*$. One can ensure that the first term is invariant under the special axial $U(1)_{\rm PQ} = U(1)_R - U(1)_L$ transformation [1] $q_L \to e^{i\alpha/2}\, q_L$, $d_R \to e^{-i\alpha/2}\, d_R$, $u_R \to e^{-i\alpha/2}\, u_R$ if one requires the Higgs field ϕ to transform as

$$\phi \to e^{i\alpha}\, \phi. \tag{2.10}$$

However, the second term in (2.9) is only invariant if ϕ_c transforms in the same way as ϕ, but this is not the case.

A simple solution is to introduce a second Higgs doublet ϕ_2 in place of ϕ_c, which is therefore independent of $\phi_1 \equiv \phi$. Then, both Higgs fields ϕ_1 and ϕ_2 transform as in (2.10), and PQ invariance of (2.9) is attained. Finally, when the $SU(2)_L \times U(1)_Y \times U(1)_{\rm PQ}$ symmetry breaks spontaneously, the massless axion appears together with three other Nambu-Goldstone bosons, which will be "eaten" by the massive $W^{\pm}$ and Z^0 gauge bosons. This is the original standard-axion model in which the breaking scale of the PQ symmetry is equal to the electroweak one, i.e. $f_a \approx 250$ GeV. The associated axion with a mass of about 100 keV, however, was quickly ruled out by experiments: if weak-scale axions were to exist, one would expect decays in the meson system like

$$K^{\pm} \to \pi^{\pm} + a\ .$$

[1] Consider a general axial transformation $U(1)_A$ and its related axial vector current $j^\mu_A = \bar{\psi}\gamma^\mu\gamma^5\psi$. With $\psi_L \equiv \frac{1}{2}(1-\gamma^5)\psi$ and $\psi_R \equiv \frac{1}{2}(1+\gamma^5)\psi$ one can write the axial current in terms of left- and right-handed currents j^μ_L and j^μ_R,

$$j^\mu_A = (\psi_R + \psi_L)\gamma^\mu\gamma^5(\psi_R + \psi_L) = \bar{\psi}_R\gamma^\mu\psi_R - \bar{\psi}_L\gamma^\mu\psi_L = j^\mu_R - j^\mu_L,$$

where we have used $\gamma^5\psi_R = \psi_R$, $\gamma^5\psi_L = -\psi_L$ and $\bar{\psi}_L\gamma^\mu\psi_R = \bar{\psi}_R\gamma^\mu\psi_L = 0$. Therefore we may write $U(1)_A = U(1)_R - U(1)_L$.

The absence of such decays implies that the standard axion can not exist. Even worse, its mass must be less than about 10 keV, or equivalently the symmetry-breaking scale must be larger than 1000 GeV.

In order to maintain the PQ solution of the strong CP problem, the "invisible axion" was invented. The special feature of these models is that the axion resides in the phase of a new complex $SU(2)_L \times U(1)_Y$ singlet scalar field Φ, which has a nontrivial PQ charge Q_Φ. As a consequence, the field Φ does not participate in weak interactions, and hence the PQ symmetry breaking is decoupled from the electroweak one. Therefore, the PQ scale f_a is an arbitrary parameter in invisible axion models, implying also that the axion's couplings are not fixed. Perhaps the most common axion models are those of Dine, Fischler, Srednicki, and Zhitnitskiĭ (DFSZ) and Kim, Shifman, Vainshtein, and Zakharov (KSVZ). The KSVZ axion is an example of a wider class of axion models, the so-called "KSVZ-type axions." The main difference between the DSVZ and KSVZ-type models is that the latter have no tree-level couplings to ordinary quarks and leptons. This is achieved by setting the PQ charge of all ordinary fermions to zero. Instead, one introduces new, heavy, colored fermions with a nonvanishing PQ charge X_f.

2.2.2 The KSVZ Model

In order to gain deeper insight into axion physics, one specific example shall be discussed in some detail, i.e. the KSVZ model. Since the KSVZ axion has no tree-level coupling to ordinary quarks, the question of whether such an axion is able to solve the strong CP problem arises: axions need an anomalous triangle coupling to two gluons, i.e. a $U(1)_{\mathrm{PQ}}$-$SU(3)_C$-$SU(3)_C$ anomaly, which is a fundamental feature of every axion model. Therefore, within the KSVZ model, one has to introduce at least one new heavy Quark $\mathcal{Q}$ with nonvanishing PQ charge and nontrivial transformation properties under $SU(3)_C$, e.g. a $SU(3)_C$ triplet. As a result, the essential $aG\tilde{G}$ coupling can be realized at lowest order via an anomalous heavy quark triangle loop, which is illustrated in Fig. 2.1.

Let us now consider the spontaneous breaking of the $U(1)_{\mathrm{PQ}}$ symmetry in the KSVZ model. To this end, we introduce a new field Φ with the associated Lagrangian

$$\begin{aligned} \mathcal{L}_\Phi &= (\partial_\mu \Phi)^\dagger (\partial^\mu \Phi) - V(\Phi) \\ &= (\partial_\mu \Phi)^\dagger (\partial^\mu \Phi) + f_{\mathrm{PQ}}^2 \Phi^\dagger \Phi - \lambda (\Phi^\dagger \Phi)^2, \end{aligned} \tag{2.11}$$

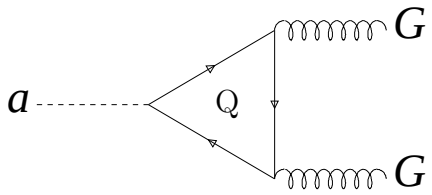

Figure 2.1: Interaction of axions with gluons via a heavy quark loop.

where $\lambda, f_{\rm PQ}^2 > 0$. Below we set $\lambda = 1$. $\mathcal{L}_\Phi$ is invariant under

$$\Phi \to e^{i\alpha}\Phi, \tag{2.12}$$

i.e. $\mathcal{L}_\Phi$ possesses a $U(1)$ global symmetry, the PQ symmetry $U(1)_{\rm PQ}$. The potential $V(\Phi)$ then has a circle of minima at $\langle\Phi\rangle = (f_{\rm PQ}/\sqrt{2})e^{i\varphi}$ with an arbitrary phase φ. Now we spontaneously break the $U(1)_{\rm PQ}$ symmetry by expanding Φ around one of these ground states $\langle\Phi\rangle$ with minimum energy. If we introduce new fields a and ρ corresponding to angular and radial excitations around $\langle\Phi\rangle$, we may write

$$\Phi = \frac{1}{\sqrt{2}}(f_{\rm PQ} + \rho)\exp\left(\frac{ia}{f_{\rm PQ}}\right). \tag{2.13}$$

The massless mode a is linked with the axion field and translates under $U(1)_{\rm PQ}$ in (2.12) as $a \to a + \alpha f_{\rm PQ}$. Now we substitute (2.13) into (2.11), i.e. we express the Lagrangian $\mathcal{L}_\Phi$ in terms of a and ρ. The result is

$$\begin{aligned}\mathcal{L}_\Phi &= \frac{1}{2}(\partial_\mu a)(\partial^\mu a) + \frac{1}{2}(\partial_\mu\rho)(\partial^\mu\rho) - f_{\rm PQ}^2\rho^2 - f_{\rm PQ}\rho^3 - \frac{\rho^4}{4} \\ &\quad + \frac{1}{f_{\rm PQ}}\rho\,(\partial_\mu a)(\partial^\mu a) + \frac{1}{2f_{\rm PQ}^2}\rho^2(\partial_\mu a)(\partial^\mu a) + \text{const.}\end{aligned} \tag{2.14}$$

The third term has the form of a mass term $(-\frac{1}{2}m_\rho^2\rho^2)$ for the ρ field. Thus, the ρ mass is $m_\rho = \sqrt{2}\,f_{\rm PQ}$. Because $f_{\rm PQ}$ is a high-energy scale, ρ is a very heavy particle and can be neglected as far as the low-energy regime is concerned. Therefore, we may keep only the axionic degree of freedom, i.e. we drop all terms involving ρ.

Finally, we have to implement the quark $\mathcal{Q}$ into our model. To this end, we add a usual Dirac term for the fermionic $\mathcal{Q}$ field and introduce Yukawa couplings between $\mathcal{Q}$ and Φ. We then write

$$\mathcal{L}_\mathcal{Q} = \frac{i}{2}\left(\bar{\mathcal{Q}}\gamma^\mu\partial_\mu\mathcal{Q} + \text{h.c.}\right) - h(\bar{\mathcal{Q}}_L\mathcal{Q}_R\,\Phi + \Phi^\dagger\bar{\mathcal{Q}}_R\mathcal{Q}_L) \tag{2.15}$$

with a Yukawa coupling constant $h > 0$. Remember, the $U(1)_{\rm PQ}$ transformation of the Φ field is already fixed through (2.12). Hence, the transformation property of the quark field $\mathcal{Q}$ is determined by the demand for $U(1)_{\rm PQ}$ invariance of the Yukawa interactions (2.15). This invariance can be achieved by

$$\mathcal{Q}_L \to e^{i\alpha/2}\mathcal{Q}_L, \qquad \mathcal{Q}_R \to e^{-i\alpha/2}\mathcal{Q}_R, \tag{2.16}$$

which is equivalent to the axial transformation $\mathcal{Q}_R + \mathcal{Q}_L \equiv \mathcal{Q} \to e^{-i\gamma^5\alpha/2}\mathcal{Q}$. Note that both $\mathcal{Q}$ and $\bar{\mathcal{Q}}$ transform in the same way, i.e. it is also $\bar{\mathcal{Q}} \to \bar{\mathcal{Q}}\, e^{-i\gamma^5\alpha/2}$. If we insert (2.13) into (2.15), we obtain for the Yukawa term, i.e. the last term in (2.15),

$$\mathcal{L}_{\rm Yuk} = -\frac{f_{\rm PQ}}{\sqrt{2}}\, h \left(\bar{\mathcal{Q}}_L \mathcal{Q}_R\, e^{ia/f_{\rm PQ}} + e^{-ia/f_{\rm PQ}}\, \bar{\mathcal{Q}}_R \mathcal{Q}_L \right), \tag{2.17}$$

where we have neglected all terms involving ρ. One can simplify this expression by using the normal field $\mathcal{Q} = \mathcal{Q}_R + \mathcal{Q}_L$ instead of the chiral quark fields $\mathcal{Q}_L$ and $\mathcal{Q}_R$. Recalling that

$$\bar{\mathcal{Q}}_L \mathcal{Q}_R = \bar{\mathcal{Q}}\, \frac{1}{2}(1+\gamma^5)\mathcal{Q} \quad \text{and} \quad \bar{\mathcal{Q}}_R \mathcal{Q}_L = \bar{\mathcal{Q}}\, \frac{1}{2}(1-\gamma^5)\mathcal{Q}, \tag{2.18}$$

one finds

$$\begin{aligned}
\mathcal{L}_{\rm Yuk} &= -\frac{f_{\rm PQ}}{\sqrt{2}}\, h\, \bar{\mathcal{Q}} \left[e^{ia/f_{\rm PQ}}\, \frac{1+\gamma^5}{2} + e^{-ia/f_{\rm PQ}}\, \frac{1-\gamma^5}{2} \right] \mathcal{Q} \\
&= -\frac{f_{\rm PQ}}{\sqrt{2}}\, h\, \bar{\mathcal{Q}} \left[\frac{e^{ia/f_{\rm PQ}} + e^{-ia/f_{\rm PQ}}}{2} + \gamma^5 \frac{e^{ia/f_{\rm PQ}} - e^{-ia/f_{\rm PQ}}}{2} \right] \mathcal{Q} \\
&= -\frac{f_{\rm PQ}}{\sqrt{2}}\, h\, \bar{\mathcal{Q}} \left[\cos(a/f_{\rm PQ}) + i\gamma^5 \sin(a/f_{\rm PQ}) \right] \mathcal{Q} \\
&= -\frac{f_{\rm PQ}}{\sqrt{2}}\, h\, \bar{\mathcal{Q}}\, e^{i\gamma^5 a/f_{\rm PQ}}\, \mathcal{Q}\ .
\end{aligned} \tag{2.19}$$

With (2.14), (2.15), and (2.19) we finally get the KSVZ Lagrangian

$$\mathcal{L}_{\rm KSVZ} = \frac{i}{2}\left(\bar{\mathcal{Q}}\gamma^\mu \partial_\mu \mathcal{Q} + \text{h.c.} \right) + \frac{1}{2}(\partial_\mu a)^2 - \frac{f_{\rm PQ}}{\sqrt{2}}\, h\, \bar{\mathcal{Q}}\, e^{i\gamma^5 a/f_{\rm PQ}}\, \mathcal{Q}\ . \tag{2.20}$$

In order to interpret the last term of this expression, we expand it in powers of $a/f_{\rm PQ}$. The zeroth-order term provides a mass for the quark $\mathcal{Q}$. Higher-order terms describe interactions between $\mathcal{Q}$ and the axion a. One obtains

$$\mathcal{L}_{\rm KSVZ} = \frac{i}{2}\left(\bar{\mathcal{Q}}\gamma^\mu \partial_\mu \mathcal{Q} + \text{h.c.} \right) + \frac{1}{2}(\partial_\mu a)^2 - \frac{f_{\rm PQ}}{\sqrt{2}}\, h\, \bar{\mathcal{Q}}\mathcal{Q} + \mathcal{L}_{\rm int}\ , \tag{2.21}$$

and thus a $\mathcal{Q}$ mass of $m_{\mathcal{Q}} = h f_{\rm PQ}/\sqrt{2}$. In addition, the interaction Lagrangian is given by

$$\mathcal{L}_{\rm int} = -i\frac{m_{\mathcal{Q}}}{f_{\rm PQ}} a \bar{\mathcal{Q}}\gamma^5 \mathcal{Q} + \frac{m_{\mathcal{Q}}}{2f_{\rm PQ}^2} a^2 \bar{\mathcal{Q}}\mathcal{Q} + \dots . \tag{2.22}$$

One then can see that to lowest order the interaction between the axion a and the exotic quark $\mathcal{Q}$ is pseudoscalar. The corresponding Yukawa coupling constant is $g_{a\mathcal{Q}} \equiv m_{\mathcal{Q}}/f_{\rm PQ}$. There are, however, higher-order terms, which sometimes must be taken into account in order to achieve the correct result. Therefore, it is better to search for an alternative approach to the a-$\mathcal{Q}$ interaction. One may remove the axion field in the Yukawa coupling term (last term in (2.20)) by a local chiral transformation of the $\mathcal{Q}$ field,

$$\mathcal{Q} \to e^{-i\gamma^5 a/2f_{\rm PQ}}\,\mathcal{Q}, \qquad \bar{\mathcal{Q}} \to e^{-i\gamma^5 a/2f_{\rm PQ}}\,\bar{\mathcal{Q}}\ . \tag{2.23}$$

With $\gamma^\mu e^{i\gamma^5\alpha} = e^{-i\gamma^5\alpha}\,\gamma^\mu$ it is straightforward to show that under (2.23) the KSVZ Lagrangian (2.20) transforms as

$$\mathcal{L}_{\rm KSVZ} \to \frac{1}{2f_{\rm PQ}}\bar{\mathcal{Q}}\gamma^\mu\gamma^5\mathcal{Q}\,\partial_\mu a + \frac{1}{2}(\partial_\mu a)^2 - m_{\mathcal{Q}}\bar{\mathcal{Q}}\mathcal{Q}\ . \tag{2.24}$$

Obviously, the transformation (2.23) generates a derivative axion interaction from the kinetic $\mathcal{Q}$ term in $\mathcal{L}_{\rm KSVZ}$ (2.20), namely

$$\mathcal{L}_{\rm int} = \frac{1}{2f_{\rm PQ}}\bar{\mathcal{Q}}\gamma^\mu\gamma^5\mathcal{Q}\,\partial_\mu a\ . \tag{2.25}$$

In contrast with (2.22), this interaction contains no higher-order terms. The existence of two different couplings

$$\mathcal{L}_{\rm int} = -i\frac{m_{\mathcal{Q}}}{f_{\rm PQ}} a \bar{\mathcal{Q}}\gamma^5\mathcal{Q} \quad \text{and} \quad \mathcal{L}_{\rm int} = \frac{1}{2f_{\rm PQ}}\bar{\mathcal{Q}}\gamma^\mu\gamma^5\mathcal{Q}\,\partial_\mu a \tag{2.26}$$

raises the question of which is to use in concrete calculations. It would be naive to suppose that both interaction Lagrangians always yield the same result because the pseudoscalar one is only the leading term of an expansion in powers of $a/f_{\rm PQ}$. Therefore, it is a safe strategy to use the derivative coupling in all calculations.

To conclude this section we finally consider the effects associated with the chiral anomaly, i.e. the axion mass. We go back to the Lagrangian (2.20) which is invariant under global $U(1)_{\rm PQ}$ transformations (2.16) and $a \to a + f_{\rm PQ}\alpha$. The associated current due to Noether's theorem is simply

$$j^\mu_{\rm PQ} = f_{\rm PQ}\partial^\mu a - \frac{1}{2}\bar{\mathcal{Q}}\gamma^\mu\gamma^5\mathcal{Q} \tag{2.27}$$

with

$$\partial_\mu j^\mu_{\rm PQ} = 0 \ . \tag{2.28}$$

However, the isosinglet axial current $\frac{1}{2}\bar{\mathcal{Q}}\gamma^\mu\gamma^5\mathcal{Q}$ has an Adler-Bell-Jackiw anomaly and is therefore not conserved at the quantum level. For the divergence of $j^\mu_{\rm PQ}$ one finds explicitly [10]

$$\partial_\mu j^\mu_{\rm PQ} = -\frac{g^2}{32\pi^2}\, G^{\mu\nu}_a\, \tilde{G}^a_{\mu\nu} \ . \tag{2.29}$$

Recall that at the scale $f_{\rm PQ}$ the PQ symmetry breaks spontaneously and the axion arises as the associated Nambu-Goldstone boson. As a result, the axion is a massless particle. However, at energies below $\Lambda_{\rm QCD}$, the axion develops a mass due to QCD effects: the heavy quark $\mathcal{Q}$ has a color anomaly. So, the axion interacts with gluons (Fig. 2.1), and therefore with quark-antiquark states. Furthermore, the axion mass should vanish in the limit of vanishing u- or d-quark masses.[2] With this information, Bardeen and Tye [11] constructed an anomaly free current $\tilde{j}^\mu_{\rm PQ}$ out of $j^\mu_{\rm PQ}$,

$$\tilde{j}^\mu_{\rm PQ} = f_{\rm PQ}\partial^\mu a - \frac{1}{2}\bar{\mathcal{Q}}\gamma^\mu\gamma^5\mathcal{Q} + \frac{1}{2}\left(\frac{m_d}{m_u+m_d}\bar{u}\gamma^\mu\gamma^5 u + \frac{m_u}{m_u+m_d}\bar{d}\gamma^\mu\gamma^5 d\right), \tag{2.30}$$

where $\bar{q}\gamma^\mu\gamma^5 q,\ q = u, d$ are the chiral quark currents. In the case that at least one quark mass vanishes, the last term of expression (2.30) is conserved up to the chiral anomaly, i.e.

$$\partial_\mu\left[\frac{1}{2}\left(\frac{m_d}{m_u+m_d}\bar{u}\gamma^\mu\gamma^5 u + \frac{m_u}{m_u+m_d}\bar{d}\gamma^\mu\gamma^5 d\right)\right] \to \frac{g^2}{32\pi^2}\, G^{\mu\nu}_a\, \tilde{G}^a_{\mu\nu} \tag{2.31}$$

for $m_u \to 0$ or $m_d \to 0$. Therefore, with (2.29), (2.30), and (2.31), it is easy to see that the Bardeen-Tye current is anomaly free and thus conserved in the limit of vanishing u- and d-quark masses,

$$\partial_\mu \tilde{j}^\mu_{\rm PQ} \to 0 \qquad \text{if} \qquad m_u \text{ or } m_d \to 0. \tag{2.32}$$

That means, the conservation law of the Bardeen-Tye current $\tilde{j}^\mu_{\rm PQ}$ is explicitly broken by nonvanishing u- and d-quark masses. This fact is referred to as the partial conservation of the axial current (PCAC). Using PCAC and the standard-current algebra approach [12], in which the axion mass is related to the "soft"

[2] Effects due to the s-quark are of order $w \equiv m_u/m_s \approx 0.029$ and are neglected for the sake of simplicity.

divergence of $\tilde{j}^{\mu}_{\mathrm{PQ}}$, the axion mass can finally be calculated as

$$m_a = \frac{f_\pi m_\pi}{f_{\mathrm{PQ}}} \frac{\sqrt{z}}{1+z} \ , \tag{2.33}$$

where $z = m_u/m_d$, $f_\pi \approx 93$ MeV the pion decay constant and $m_\pi = 135$ MeV the pion mass.

2.3 General Axion Couplings

For the most part, axion physics is determined by the scale f_a of PQ symmetry breaking. According to (2.8), the axion's couplings to photons and fermions are all proportional to the inverse PQ symmetry breaking scale or, equivalently, to the axion mass

$$\text{Axion-Couplings} \sim \frac{1}{f_a} \propto m_a \ .$$

In detail, however, these couplings are model dependent, i.e. they depend on the implementation of the PQ mechanism.

2.3.1 Photons

First we consider the axion's coupling to photons. An apparent reason for this interaction is the axion-pion mixing: As a result of the electromagnetic anomaly, pions couple to two photons, causing an effective axion-photon coupling. Over and above that, there is a second contribution to the axion-photon interaction. In general, the axion has Yukawa couplings to fermions which carry PQ charges. If these PQ fermions also carry electric charges, they couple the axion to two photons by means of a triangle loop (Fig. 2.2). As a consequence of the axion-photon coupling, axions decay into two photons with a lifetime

$$\tau_{a\gamma\gamma} \ = \ \left[\frac{\alpha^2 m_a^3}{256\pi^3 f_a^2} \, C_{a\gamma\gamma}^2 \right]^{-1}$$

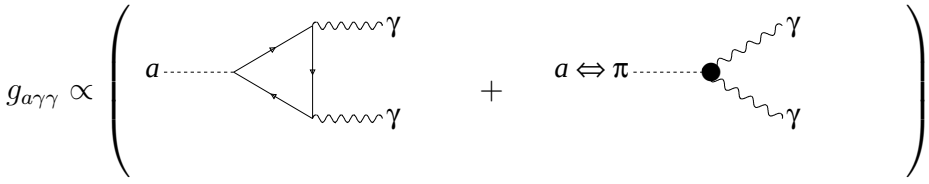

Figure 2.2: Coupling of the axion to two photons. The left triangle loop is made up of fermions carrying PQ and electric charge

$$= \quad 3.53 \times 10^{24} \text{ sec } m_{\text{eV}}^{-5} \, C_{a\gamma\gamma}^{-2} \ , \tag{2.34}$$

where $\alpha = 1/137$ is the fine-structure constant.

Let us now study some characteristic properties of the axion-photon coupling. If we demand CP-invariance, the effective Lagrangian for the axion-photon interaction can be written as

$$\mathcal{L}_{a\gamma\gamma} = -\frac{1}{4} g_{a\gamma\gamma} F_{\mu\nu} \tilde{F}^{\mu\nu} a = g_{a\gamma\gamma} \, a \, \mathbf{E} \cdot \mathbf{B} \ , \tag{2.35}$$

where F is the electromagnetic field strength tensor, $\tilde{F}$ its dual, a the pseudoscalar axion field, and $g_{a\gamma\gamma}$ the axion-photon coupling strength with the dimension (energy)$^{-1}$. The latter is given by

$$g_{a\gamma\gamma} = \frac{\alpha}{2\pi f_a} \left[\frac{E}{N} - \frac{2(4+z+w)}{3(1+z+w)} \right], \tag{2.36}$$

where $\alpha = 1/137$ is the fine structure constant, E the electromagnetic anomaly, and N the color anomaly of the PQ symmetry. They are given by

$$N \equiv \sum_j X_j, \qquad E \equiv 2 \sum_j X_j \, Q_j^2 \, D_j \ , \tag{2.37}$$

where X_j and Q_j are the PQ charges and the electric charges of the PQ fermions, respectively, and $D_j = 1$ for color singlets (charged leptons) and 3 for color triplets (quarks). Finally, z and w are the mass ratios of the u- to the d-quark and the u- to the s-quark, respectively. The first term of expression (2.36) corresponds to the electromagnetic anomaly of the PQ fermions, whereas the second term is associated with the axion-pion mixing.

From (2.36) it is clear that the light quark mass ratios z and w are of great interest, since they determine the axion-photon coupling strength $g_{a\gamma\gamma}$. However, even though there has been considerable effort to calculate the numerical values for z and w, the results are still controversial and remain under active discussion. Leutwyler [13] used chiral perturbation theory results for the kaon and pion masses and extracted from those the relative sizes of m_u, m_d, and m_s. He obtained the very stringent constraints

$$\begin{aligned} z \ &\equiv \ m_u/m_d \ \approxeq \ 0.553 \pm 0.043 \\ w \ &\equiv \ m_u/m_s \ \approxeq \ 0.029 \pm 0.003 \ . \end{aligned} \tag{2.38}$$

However, alternative approaches have been made, e.g. using sum rules and numerical simulations of QCD on a lattice. These calculations lead to different results

which are not mutually consistent. Therefore, it remains to be seen whether the results (2.38) are reliable. The Particle Data Group gives the conservative range $z = 0.2$–0.7 [14]. Therefore, we rather use

$$z \approx 0.55 \pm 0.1 \tag{2.39}$$

than the z-values of expression (2.38). With (2.7) and (2.39), we finally obtain the axion-photon coupling in terms of the axion mass,

$$\begin{aligned} g_{a\gamma\gamma} &= \frac{\alpha}{2\pi f_a}\left(\frac{E}{N} - 1.93 \pm 0.08\right) \\ &= \frac{m_{\rm eV}}{0.52\times 10^{10}\ {\rm GeV}}\left(\frac{E}{N} - 1.93 \pm 0.08\right), \end{aligned} \tag{2.40}$$

where have used $m_{\rm eV} \equiv m_a/{\rm eV}$ and (2.38). Hereafter we use the abbreviation

$$C_{a\gamma\gamma} \equiv \frac{E}{N} - 1.93\ . \tag{2.41}$$

In the DSVZ model and grand unified theory (GUT) models one has $E/N = 8/3$. This implies $(E/N - 1.93) \approx 0.75$.

However, in the KSVZ model one finds $E/N = 6\,Q_{\rm em}$, where $Q_{\rm em}$ is the electric charge of the heavy quark $\mathcal{Q}$. Moreover, in more general KSVZ-type models the number N of heavy quarks and their transformation properties under $SU(3)_C$ are arbitrary. Therefore, as Kaplan [6] first pointed out, it is possible to construct KSVZ-type models with $E/N = 2$, leading to a very small $C_{a\gamma\gamma}$. In the light of the considerable uncertainties of the light-quark ratios w and z, it is even possible that $C_{a\gamma\gamma} = 0$. We will see in Chapter 3 that KSVZ-type axions with an accidentally suppressed photon coupling and masses between 10 and 20 eV are astrophysically allowed, particles which we refer to as "hadronic axions."

2.3.2 Electrons

Tree-Level Coupling to Electrons:

In many axion models ordinary electrons carry PQ charges and have fundamental Yukawa couplings to the Higgs field. Then the tree-level coupling between axions and electrons has the structure of expression (2.26). The associated coupling constant is

$$g_{ae}^{\rm tree} = \frac{C_e m_e}{f_a} = C_e\ 0.85\times 10^{-10}\, m_{\rm eV}, \tag{2.42}$$

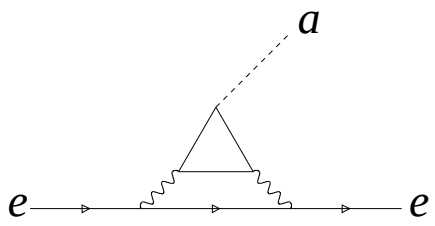

Figure 2.3: Radiatively induced axion-electron coupling.

where $C_e = X'_e/N$ is a numerical coefficient of order unity. Here, X'_e is the shifted PQ charge of the electron [15], and N the color anomaly. Of course, in KSVZ-type models one has $C_e = 0$.

Radiatively Induced Coupling to Electrons:

In addition to the tree-level coupling, there exists a loop correction due to the axion's interaction with photons (Fig. 2.3). Such a radiatively induced coupling exists even if $X'_e = 0$. This loop correction can be described by the effective coupling constant [15]

$$g_{ae}^{\rm loop} = \frac{3\alpha^2}{4\pi^2}\frac{m_e}{f_a}\left[\frac{E}{N}\ln\left(\frac{f_a}{m_e}\right) - \frac{2(4+z+w)}{3(1+z+w)}\ln\left(\frac{\Lambda_{\rm QCD}}{m_e}\right)\right] \tag{2.43}$$

with the cut-off scales f_a and $\Lambda_{\rm QCD} \approx 150$–$400$ MeV, respectively.

Considering both the tree-level and the radiatively induced coupling, we obtain for the total axion-electron interaction Lagrangian

$$\begin{aligned}\mathcal{L}_{ae} &= -i\left(g_{ae}^{\rm tree} + g_{ae}^{\rm loop}\right)\bar\psi_e\gamma_5\psi_e a \qquad (2.44)\\ &= -i\frac{m_e}{f_a}\left\{C_e + \frac{3\alpha^2}{4\pi^2}\left[\frac{E}{N}\ln\left(\frac{f_a}{m_e}\right) - \frac{2(4+z+w)}{3(1+z+w)}\ln\left(\frac{\Lambda_{\rm QCD}}{m_e}\right)\right]\right\}\\ &\quad\times\bar\psi_e\gamma_5\psi_e a\ .\end{aligned}$$

Although the loop correction is of $\mathcal{O}(\alpha^2)$ smaller than the tree-level result, it is particularly important for KSVZ-type axions because they have $g_{ae}^{\rm tree} = 0$. In this case, one is left with the radiative coupling (2.43) or, numerically,

$$g_{ae}^{\rm loop} \approx 3.4\times10^{-16}\ m_{\rm eV}\left[\frac{E}{N}\left(23.2 - \ln m_{\rm eV}\right) - 12\right]. \tag{2.45}$$

For hadronic axions with $E/N \approx 2$ this is $g_{ae}^{\rm loop} \approx 10^{-14}\, m_{\rm eV}$.

2.3.3 Nucleons

Naturally, if ordinary quarks carry PQ charges they have fundamental Yukawa couplings to axions. But in astrophysical considerations one is confronted with energies below the QCD scale $\Lambda_{\rm QCD} \approx 150$–$400$ MeV. Thus, free quarks do not exist and one is interested in the effective coupling of axions to nucleons. This interaction arises from two roughly equal contributions. First, there is the tree-level coupling of axions to up and down quarks. Moreover, the familiar axion-pion mixing provides a second term for the axion-nucleon interaction. The resulting effective axion-nucleon interaction can be described by a Lagrangian similar to that of (2.26). The axion-nucleon coupling constant is defined as

$$g_{aN} = \frac{C_N m_N}{f_a}, \tag{2.46}$$

where C_N is the effective PQ charge of the nucleon. This charge C_N is a compound parameter combining both parts of the axion-nucleon interaction, i.e. the tree-level part and the part due to the axion's mixing with pions. For neutrons and protons it is

$$\begin{aligned} C_p &= (C_u - \eta)\Delta u + (C_d - \eta z)\Delta d + (C_s - \eta w)\Delta s \ , \\ C_n &= (C_u - \eta)\Delta d + (C_d - \eta z)\Delta u + (C_d - \eta w)\Delta s \ , \end{aligned} \tag{2.47}$$

where $\eta \equiv (1+z+w)^{-1} = 0.632$ with $z \equiv m_u/m_d$ and $w \equiv m_u/m_s$. Furthermore, Δq describes the fraction of the nucleon's spin carried by the quark flavour q. Numerically, one finds [16]

$$\begin{aligned} \Delta u &= +0.80 \pm 0.04 \pm 0.04 \, , \\ \Delta d &= -0.46 \pm 0.04 \pm 0.04 \, , \\ \Delta s &= -0.12 \pm 0.04 \pm 0.04 \, , \end{aligned} \tag{2.48}$$

where the first error is statistical, and the second is of systematic nature.

Let us now consider KSVZ-type axions in more detail. In spite of their vanishing couplings to ordinary quarks, their interaction with nucleons is not zero. Actually, the axion-nucleon coupling of KSVZ-type axions is comparable to that which appears in models with existing tree-level coupling to quarks, e.g. the DFSZ model. The fundamental reason is the generic axion-pion mixing which exists even though the tree-level coupling to quarks vanishes. With vanishing PQ

charges C_u, C_d, and C_s of the u-, d-, and s-quarks, respectively, and with (2.47) one obtains explicitly

$$C_p = -0.34 \quad \text{and} \quad C_n = 0.01. \tag{2.49}$$

These values imply

$$\begin{aligned} g_{ap} &= \frac{C_p m_p}{f_a} = -5.32 \times 10^{-8}\, m_{\rm eV}\ , \\ g_{an} &= \frac{C_n m_n}{f_a} = 1.57 \times 10^{-9}\, m_{\rm eV} \end{aligned} \tag{2.50}$$

for the KSVZ Yukawa couplings.

Chapter 3

Hadronic Axion Bounds

Present bounds on the hadronic axions are reviewed; for more general models see [5]. The possibility of novel hadronic axion bounds, based on neutron star cooling and accretion discs around black holes, is deferred to Chapter 6. Limits on f_a (or m_a) are usually based on limits on the coupling strength to photons, electrons, and nucleons. These limits, in turn, are derived from astrophysical objects like the sun or white dwarfs where axion production would increase stellar energy losses and thus modify the observed properties of stars ("energy-loss argument"). For hadronic axions the relevant astrophysical objects are mainly globular cluster stars and SN 1987A.

3.1 Globular Clusters

All stars in a globular cluster have nearly the same age and equal chemical properties; they differ primarily in one single parameter, their initial mass. Particularly interesting for axions are two different kinds of stars, namely those occupying the red-giant branch (RGB) and the horizontal branch (HB). The main characteristic of the former is their degenerate helium core, whereas the latter are characterized by a helium-burning core. In both kinds of stars the core is surrounded by a hydrogen burning shell. In the interior of HB and RGB stars axions could be produced by different mechanisms, leading to bounds on the axion-photon and the axion-electron coupling.

3.1.1 Photon Coupling

In globular-cluster stars photons can be transformed into axions by means of the axion-two photon interaction. This effect is referred to as Primakoff conversion. It takes place in both the HB and RGB star cores, but, as a consequence of the different core densities, Primakoff conversion is much more effective in HB stars. Therefore, an additional axionic energy loss would shorten the lifetime of HB stars, leading to a reduced HB/RGB number ratio, in contradiction to observations. These considerations lead to the bound [17]

$$g_{a\gamma\gamma} \lesssim 0.6 \times 10^{-10}\ \mathrm{GeV}^{-1}\ . \tag{3.1}$$

With (2.40) one obtains

$$C_{a\gamma\gamma}\, m_{\mathrm{eV}} \lesssim 0.3\ , \tag{3.2}$$

where again $m_{\mathrm{eV}} = m_a/\mathrm{eV}$ and $C_{a\gamma\gamma} = (E/N - 1.93)$. Obviously, the limits on $C_{a\gamma\gamma}$ and m_a are not independent. In particular, for hadronic axions we have $C_{a\gamma\gamma} \ll 1$, and no meaningful limit on m_a may be derived.

3.1.2 Electron Coupling

Another constraint may be obtained by considering the axionic energy loss via the bremsstrahlung process $e^- + (A, Z) \to e^- + (A, Z) + a$. The consequence of this energyloss would be a delay of the helium flash in the red-giant core, resulting in a greater core mass at helium ignition. A comparison between the predicted and observed core masses at the helium flash yields [17]

$$g_{ae} \lesssim 2.5 \times 10^{-13}\ . \tag{3.3}$$

In the case of hadronic axions, g_{ae} is given by the radiatively induced coupling, implying the condition

$$m_{\mathrm{eV}}(C_{a\gamma\gamma} + 1.3) \lesssim 35. \tag{3.4}$$

As a result of the SN 1987A bound, which will be discussed below, the mass of hadronic axions is restricted to the range between 10 and 20 eV. This requires $C_{a\gamma\gamma}$ to be less than 0.45–2.2, which can be easily provided in KSVZ-type models.

3.2 SN 1987A

Axions could be produced via nucleon-nucleon axion bremsstrahlung $N + N \to N+N+a$ in the core of a supernova. As a consequence, the most important bound

on hadronic axion masses can be derived from the SN 1987A by considering the strength and duration of the observed neutrino signal at the Kamiokande II (KII) and the Irvine-Michigan-Brookhaven (IMB) water-Cherenkov detectors. Depending on their masses m_a, axions either escape freely or are radiated from an axion sphere. This energy loss can have three different observable effects: first, it can significantly shorten the observed neutrino burst, second, it can cause additional counts in the neutrino detectors, and finally, emitted axions could alter the extragalactic background light via their radiative decay.

3.2.1 Nucleon Coupling

Axions produced in the SN core compete with the standard neutrino cooling channel, i.e. they remove energy from the neutrino signal, implying a shortening of the observed neutrino signal. The axion luminosity L_a depends on the axion-nucleon coupling g_{aN} and therefore indirectly on the axion mass m_a. Assuming that the mean free path of axions is larger than the size of the core, axions are able to escape freely. In this instance the axion luminosity L_a increases with increasing axion mass: the greater m_a, the stronger g_{aN}, and thus the axion emission rate. On the other hand, if axions interact too strongly, they are trapped inside the core and are emitted from an axion sphere, similar to the well-known concept of a neutrino sphere. A simple analytical model [18, 19] showed that the axion luminosity in the trapped regime varies as $L_a \propto m_a^{-16/11}$, i.e. L_a decreases with increasing axion mass m_a. Naturally, beyond some large coupling g_{aN}, axions will be trapped so effectively that their impact on the SN cooling is again negligible. Summarizing these arguments, we can conclude that axions must either couple sufficiently weakly or sufficiently strongly to nucleons to avoid a conflict with the observed neutrino signals at KII and IMB. Accurate calculations [20, 16, 17] yield the excluded range

$$3 \times 10^{-10} \lesssim g_{aN} \lesssim 3 \times 10^{-7} \ . \tag{3.5}$$

Assuming a proton fraction of 0.3 inside the SN core, one can calculate an effective axion-nucleon coupling $C_{aN} \equiv \sqrt{0.3C_{ap}^2 + 0.7C_{an}^2} \approx 0.2$, where we have used (2.49). With $g_{aN} = C_N m_N / f_a$ one finally obtains

$$\begin{aligned} 0.01 \text{ eV} \lesssim \quad & m_a \quad \lesssim 10 \text{ eV} \ , \\ 6 \times 10^8 \text{ MeV} \lesssim \quad & f_a \quad \lesssim 6 \times 10^{11} \text{ MeV} \end{aligned} \tag{3.6}$$

for the SN 1987A exclusion parameters of hadronic axions.

But even axions which are allowed by the energy-loss argument can have measurable effects, as they might produce additional counts in the water-Cherenkov detectors. Engel et al. [21] showed that such heavy hadronic axions are able to induce nuclear excitations in oxygen, $a + {}^{16}\mathrm{O} \to {}^{16}\mathrm{O}^*$. After that, nuclear deexcitations produce γ-rays which can then be detected. Hence, one can estimate a range between

$$\begin{aligned} 20 \text{ eV} \lesssim \quad & m_a \quad \lesssim 20 \text{ keV} , \\ 3 \times 10^5 \text{ MeV} \lesssim \quad & f_a \quad \lesssim 3 \times 10^8 \text{ MeV} \end{aligned} \tag{3.7}$$

for excluded hadronic axion masses.

3.2.2 Photon Coupling

If axions had been emitted from SN 1987A, they might have produced a flux of γ-rays due to their radiative decay mode $a \to 2\gamma$. Hadronic axions with $m_a \sim 10$ eV should have been emitted with a fluence of approximately $f_a \approx 5.7 \times 10^{10}\, m_{\mathrm{eV}}^{-12/11}$ cm^{-2} [18]. On condition that the axion-photon coupling $g_{a\gamma\gamma}$ is strong enough, the resulting γ-fluence f_γ could have been detected by the gamma-ray spectrometer (GRS) on the Solar Maximum Mission (SMM) satellite. The fact that the GRS did not detect any signal above the instrument background sets an upper limit to the expected γ-fluence f_γ [17, 22],

$$f_\gamma \approx 10^{-9}\, C_{a\gamma\gamma}^2 m_a^{58/11} \lesssim 0.4 . \tag{3.8}$$

The SN 1987A bound derived in the previous section precludes axion masses smaller than 10 eV and greater than 20 eV. Therefore, if we use 20 eV as a maximum value for the mass we obtain the conservative limit

$$C_{a\gamma\gamma} \lesssim 7, \tag{3.9}$$

which is less stringent than (3.2).

3.3 Gamma-Ray Background Limits

Nontrivial constraints come from the axionic contribution to the extragalactic background light. As we will see in Chapter 4, hadronic axions could have been produced in the early universe. These relic axions could have left their mark due

their radiative decay mode $a \to 2\gamma$, provided that the axion-photon coupling $g_{a\gamma\gamma}$ is sufficiently strong.

Overduin and Wesson [23] considered the diffuse extragalactic background light and searched for axion-decay photons. The absence of a signal implies

$$C_{a\gamma\gamma} < 0.323,\, 0.05,\, 0.015 \quad \text{for axion masses} \quad m_{\rm eV} = 5.3,\, 8.6,\, 13\ . \tag{3.10}$$

These limits give strong constraints on the axion-photon coupling, but they can be fulfilled assuming an accidental cancellation $C_{a\gamma\gamma} = 0$.

Furthermore, Ressel [24] searched for photon emission lines in the center of three clusters of galaxies, i.e. he considered the flux from a particular region of the sky rather than the whole sky. He obtained the bounds $C_{a\gamma\gamma} < 0.12$, 0.059, 0.029, 0.024, 0.012, and 0.008 for $m_{\rm eV} = 3.5$, 4.0, 4.5, 5.0, 6.0, and 7.5, respectively. However, masses less then 10 eV are already ruled out as a consequence of the energy loss argument applied to SN 1987A.

3.4 Big Bang Nucleosynthesis (BBN)

The bounds of the previous sections have been frequently discussed so that we just gave a brief summary. However, the possible impact of hadronic axions on BBN has not been investigated in such detail, justifying a closer look.

It will be shown in the next chapter that hadronic axions with masses $m_a =$ 10–20 eV would have come into thermal equilibrium after the quark-hadron phase transition. At temperature $T_D \sim 60$ MeV they decouple and are thus highly relativistic. The fact that hadronic axions might have an energy density ρ_a comparable to that of a light neutrino species would affect the outcome of BBN which takes place at about 0.05 MeV. During that epoch the universe is radiation dominated, and the expansion rate H depends on the total energy density ρ according to the Friedmann equation,

$$H^2 \equiv \left(\frac{\dot{R}}{R}\right)^2 = \frac{8\pi}{3} G_N \rho. \tag{3.11}$$

If one takes the existence of relativistic axions at $T \approx 1$ MeV into account, the expansion parameter is increased due to the axion's energy density ρ_a. An increase of H means that the all-important neutron-proton ratio n/p, which is regulated by the weak interactions, freezes out at an earlier time, when n/p was

larger. Therefore, taking hadronic axions into account, more ^{4}He is synthesized than in the standard scenario.

In order to estimate the influence of thermally produced hadronic axions on BBN, one compares their energy density ρ_a with that of a light neutrino species, e.g. the electron neutrino. Both particles are relativistic so that

$$\Delta N \equiv \left(\frac{\rho_a}{\rho_\nu}\right) = \frac{4}{7}\left(\frac{T_a}{T_\nu}\right)^4, \tag{3.12}$$

where the factor 4/7 is due to different phase-space distributions and different spins of neutrinos and axions. This equation means that the axion's energy density is equivalent to an effective number ΔN of additional light neutrinos. When axions decouple at $T_D \sim 60$ MeV, T_a equals T_ν and thus $\Delta N = 4/7$. Below T_D the axion temperature scales as $T_a \propto R^{-1}$. The light neutrino decouples later at $T \approx 1$ MeV and $g_* T_\nu^3 R^3$ remains constant. In the standard scenario, the total number of effective, relativistic spin degrees of freedom does not change until BBN takes place, so that $T_n u \propto R^{-1}$. Therefore, we obtain for ΔN at the time of BBN

$$\Delta N_{\rm BBN} \equiv \left(\frac{\rho_a}{\rho_\nu}\right)\Bigg|_{T=T_{\rm NS}} = \frac{4}{7}. \tag{3.13}$$

This result has now to be compared with the standard model of BBN, something that turns out to be anything but simple: In accordance with the standard BBN scenario, the mass fraction of helium, conventionally referred to as $\mathrm{Y_p}(^4\mathrm{He})$, depends not only on $N_{\rm BBN}$ but also on the uncertainties of the baryon-to-photon ratio $\eta \equiv n_B/n_\gamma$. The predicted helium abundance must then be compared with the observed ^{4}He abundance, a quantity that is difficult to estimate, implying that an upper constraint on $\Delta N_{\rm BBN}$ is afflicted with significant uncertainties. Different authors obtain different results: Olive et al. [25] found the restrictive limit of $\Delta N_{\rm BBN} \leq 0.3$. However, Kernan and Sarkar [26] provide the conservative bound $\Delta N_{\rm BBN} \leq 1.53$. If we use that value, no danger is ahead as far as hadronic axions are concerned because our result (3.13) is within the above constraint. A review of BBN, $\Delta N_{\rm BBN}$-limits and related issues can be found in [27]. In a nutshell, due to the lack of reliable data, it is premature to infer from BBN-based arguments that a hadronic axion with $f_a \sim 10^6$ GeV can not exist.

3.5 The Hadronic Axion Window

In summary, there is a gap of allowed axion masses between 10 and 20 eV. This is a result of the fact that the two different SN 1987A exclusion regions—on the one hand the "too much energy loss" region (3.6), on the other the "too many events in detectors" region (3.7)—do not overlap. This 10–20 eV window is open because the globular-cluster bounds (3.1), (3.4), and the γ-ray background observation limits (3.10) are of no importance if $C_{a\gamma\gamma}$ is accidentally suppressed. According to our discussion in Sect. 2.3.1 this is well possible. Consequently, we are not able to rule out KSVZ-type axions with a strictly suppressed coupling to photons.

Chapter 4

Relic Axions

Thermal production of hadronic axions in the early universe is discussed. We show that these particles are highly relativistic when they freeze out, implying that hadronic axions behave like HDM. Moreover, we estimate the present axion density and find that it is comparable with that required in mixed dark matter scenarios.

4.1 Thermal Production in the Early Universe

If axions were produced in the early universe, they could constitute dark matter. In principle, there are two different production mechanisms. First, axions can arise as a result of the usual "freeze out process." However, this thermal production is only meaningful if the axion couplings are sufficiently strong, implying that m_a must be greater than several 10^{-2} eV [28]. Furthermore, there are two non-thermal production mechanisms, according to different cosmological scenarios: If inflation occurred after the PQ symmetry breaking or if $T_{\rm reheat} < f_a$, axions are produced by means of the "misalignment mechanism." Before the QCD phase transition, the parameter $\bar{\Theta}$ is not at its CP-conserving minimum $\bar{\Theta} = 0$, but somewhere between 0 and π. Later, at a temperature around $T \sim \Lambda_{\rm QCD}$, the $\bar{\Theta}$-field rolls toward $\bar{\Theta} = 0$, resulting in coherent oscillations which correspond to a condensate of zero-momentum axions. On the other hand, if the universe did not inflate at all or if inflation occurred before the PQ symmetry breaking with $T_{\rm reheat} > f_a$, a network of cosmic axion strings forms at $T \sim f_a$ by the Kibble mechanism, gradually decaying into (massless) axions. At lower temperature $T \sim \Lambda_{\rm QCD}$, these axions acquire a small mass and become nonrelativistic.

As a consequence of the axion's Nambu-Goldstone nature, both the misalignment and the string-decay picture predict that the axion energy density ρ_a is proportional to $m_a^{-1.175}$, implying a lower limit on the axion mass around 10^{-3} eV. Moreover, in the mass range between approximately 10^{-5} and 10^{-3} eV, nonthermally produced axions would be an ideal candidate for CDM. However, due to unknown initial conditions on $\bar{\Theta}$, and uncertainties in the quantitative treatment of the string mechanism, the axion mass density ρ_a is not straightforward to calculate so that the function $Omega(m_a)$ remains uncertain.

In this work we are mainly concerned with hadronic axions. For these particles, the nonthermal production takes place at a temperature where the axions are still in contact with the thermal bath of the universe, implying that nonthermal mechanisms do not take place. Therefore, we will now focus on the thermal production of hadronic axions.

The interactions of axions with the thermal bath are all of the general form

$$a + X_1 \leftrightarrow X_2 + X_3, \tag{4.1}$$

where X_i, i =1, 2, 3 are particles of the primordial heat bath. Then, axion production is described by the covariant Boltzmann equation, and we may write for the number of axions in a comoving volume $Y = n_a/s$ [29]

$$\frac{dY}{dx} = -\frac{\Gamma_{\text{abs}}}{xH}\,(Y - Y_{\text{EQ}}), \tag{4.2}$$

where $Y_{\text{EQ}} = n_a^{\text{EQ}}/s$ is the equilibrium number of axions in a comoving volume, H the expansion rate of the universe, and $\Gamma_{\text{abs}} = n_1\langle\sigma v\rangle$ is the thermal averaged axion absorption rate of the process (4.1). Furthermore, $s = S/R^3 = (2\pi^2/45)g_*T^3$ is the entropy density, where g_* is the total number of effective spin degrees of freedom of all relativistic bosons and fermions that are in thermal equilibrium at the given temperature. Finally, we used the scaling parameter $x \equiv m_N/T$ with the nucleon mass m_N and the ambient temperature T.

Axions decouple from the thermal bath when Y does not change anymore, i.e $dY/dx \approx 0$. According to equation (4.2), this freeze out happens when the ratio Γ_{abs}/H becomes small, $\Gamma_{\text{abs}} \lesssim H$. Let us now estimate the decoupling temperature T_D for hadronic axions, i.e. the temperature T_D at which $\Gamma_{\text{abs}} \approx H$. Under the assumption $T < \Lambda_{QCD} \approx 300$ MeV nucleons already exist in the universe and a possible realization of (4.1) is the axion-pion conversion

$$a + N \leftrightarrow \pi + N. \tag{4.3}$$

With the couplings $g_{aN} = m_N/f_a$, $g_{\pi N} \approx m_\pi^{-1}$, and a factor m_N^{-1} for the nonrelativistic nucleon propagator one can estimate the interaction cross section for this process

$$\langle \sigma v \rangle \approx \left(\frac{m_N}{f_a} \frac{1}{m_\pi} \frac{1}{m_N} T \right)^2 = \frac{T^2}{f_a^2\, m_\pi^2} \tag{4.4}$$

and therefore

$$\Gamma_{\rm abs} = n_N \langle \sigma v \rangle \approx \frac{n_N T^2}{f_a^2\, m_\pi^2}\ . \tag{4.5}$$

In the case of nonrelativistic nucleons with a chemical potential $\mu \ll T$ the number density is given by $n_N \approx (m_N T)^{3/2}\, e^{-x}$. Furthermore, in the radiation dominated early universe one has

$$H = 1.67\, g_*^{1/2} \frac{m_N^2}{m_{\rm Pl}\, x^2}, \tag{4.6}$$

where $m_{\rm Pl}$ is the Planck mass. For the relevant temperatures, the particles contributing to g_* are γ, e^+, e^-, ν_e, ν_μ, ν_τ, $\bar\nu_e$, $\bar\nu_\mu$, $\bar\nu_\tau$, and a, implying $g_* = 11.75$ so that we obtain

$$\frac{\Gamma_{\rm abs}}{H} \approx 0.60\, \frac{m_N^3\, m_{\rm Pl}}{f_a^2\, m_\pi^2\, g_*^{1/2}}\, x^{-3/2} e^{-x} \approx 2.7 \times 10^6\, m_{\rm eV}^2\, x^{-3/2} e^{-x}\ , \tag{4.7}$$

with $m_{\rm eV} \equiv m_a/{\rm eV}$. The decoupling temperature T_D is reached when this ratio equals 1. Fig. 4.1 shows T_D as a function of hadronic axion masses between 10 eV and 20 eV, i.e. for the parameter range of the hadronic axion window. We see that the decoupling temperature is approximately

$$T_D \approx 57\text{–}61\ {\rm MeV}\ . \tag{4.8}$$

Although this calculation was only a rough estimate, there is no doubt that hadronic axions are highly relativistic when they freeze out. Hence, their equilibrium number density is $n_a = \zeta(3) T^3/\pi^2$ so that we find

$$Y_{\rm EQ} = \frac{n_a^{EQ}}{s} = \frac{45\, \zeta(3)}{2\pi^4} \frac{1}{g_*} \approx 0.024 \tag{4.9}$$

for the equilibrium number per comoving volume. To estimate the present abundance of relic axions, we return to the Boltzmann equation (4.2) which can be solved easily because $Y_{\rm EQ}$ is constant. With the boundary condition $Y(0) = 0$, i.e. initially no axions were present, one finds

$$Y(x) = Y_{EQ} \left(1 - \exp\left[- \int_0^x \frac{\Gamma_{\rm abs}}{x' H} dx' \right] \right). \tag{4.10}$$

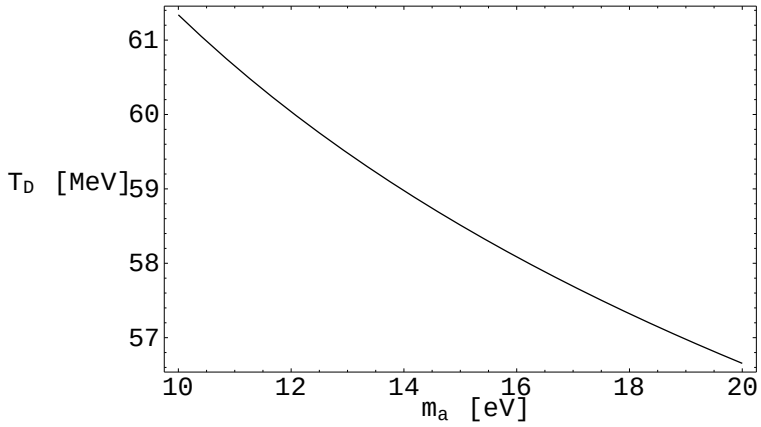

Figure 4.1: Decoupling temperature T_D of hadronic axions as a function of their mass m_a.

Strictly speaking, we would have to integrate from the very beginning ($x = 0$) to the present ($x = x_{\rm today} \equiv x_0$) to find the number of axions in the universe. However, today axions are decoupled, and the present ratio $\Gamma_{\rm abs}/H$ in (4.10) is extremely small. Thus we may integrate forward to $x = \infty$ rather then to $x = x_0$. Moreover, we are interested in the time after the QCD phase transition which occurs roughly at $x_{\rm QCD} \equiv m_N/\Lambda_{\rm QCD} \approx 5$ so that

$$Y(x_0) = Y_{EQ}\left(1 - \exp\left[-\int_{x_{\rm QCD}}^{\infty} \frac{\Gamma_{\rm abs}}{x' H} dx'\right]\right). \tag{4.11}$$

Together with expression (4.7) and hadronic axion masses $m_a = \mathcal{O}(10\ \text{eV})$, it is easy to see that the exponential function $\exp[-\int \ldots]$ can be neglected. Hence we find that the present number of axions per comoving volume is identical with its value at freeze out, i.e.

$$Y(x_0) = Y_{\rm EQ}(x_D) \approx 0.024. \tag{4.12}$$

Now we can calculate the present number density n_a^0 of relic hadronic axions. With $s_0 = 2970\ \text{cm}^{-3}$ for the present entropy density, we find

$$n_a^0 = Y(x_0)\, s_0 \approx 71\ \text{cm}^{-3}\ . \tag{4.13}$$

One can compare this result with the number density $n_\nu^0 = 115\ \text{cm}^{-3}$ of relic electron neutrinos and obtains

$$\left(\frac{n_a^0}{n_\nu^0}\right) \approx 0.6. \tag{4.14}$$

Our calculation of the hadronic axion decoupling temperature (4.8) and its present number density, (4.13) or (4.14), is just an estimate because we have only considered the axion-pion conversion process $a + N \leftrightarrow \pi + N$. A more careful approach includes an accurate computation of all relevant processes. First, these are the reactions

$$\pi^0 n \leftrightarrow an,\ \pi^0 p \leftrightarrow ap,\ \pi^+ n \leftrightarrow ap,\ \pi^- p \leftrightarrow an. \tag{4.15}$$

In addition, there are reactions involving only pions rather than nucleons and pions,

$$\pi^+\pi^- \leftrightarrow a\pi^0,\ \pi^0\pi^\pm \leftrightarrow a\pi^\pm. \tag{4.16}$$

These processes were evaluated by Chang and Choi [30]. They assert that the pure pion processes (4.16) dominate over the mixed ones (4.15) for temperatures up to 150 MeV, which is above our estimated decoupling temperature $T_D \sim 60$ MeV. Therefore, the total interaction rate including all relevant processes is greater than our approximation, implying that the ratio Γ/H equals 1 at lower temperatures, i.e. axion decoupling occurs at temperatures below $T_D \sim 60$ MeV. In fact, Chang and Choi found $T_D \approx 30$–50 MeV. However, axions are relativistic particles when they freeze out, and thus the present number density n_a^0 of relic axions is quite insensitive to the exact value of the decoupling temperature. The reason is that n_a^0 in (4.13) depends only slightly upon T_D, through $g_*|_{x=x_D}$. However, both for $T_D \sim 60$ MeV and $T_D \approx 30$–50 MeV, the effective number of spin degrees of freedom g_* is given by 11.75. Therefore, our estimate (4.12) agrees with the exact calculation taking all interaction processes into account, which yields $Y(x_0) \cong 0.02$ [4].

4.2 Hadronic Axions as Hot Dark Matter

The existence of thermally produced hadronic axions, which are highly relativistic when they freeze out, means that these particles contribute to cosmic hot dark matter (HDM). The present hadronic axion number density (4.13) can be translated into the axion contribution to the present mass density, one obtains

$$\Omega_{\rm HDM}\, h^2 = 0.007\, m_{\rm eV}, \tag{4.17}$$

where h is the Hubble constant H_0 in units of 100 km sec^{-1} Mpc^{-1}. Numerically, one finds with $h \approx 0.6$–0.8 and $m_a \approx 10$–20 eV

$$\Omega_{\rm HDM} \approx 0.1\text{–}0.4. \tag{4.18}$$

This is the right ballpark for a HDM component required in mixed dark matter scenarios, [31, 32].

Chapter 5

Axions in a Nuclear Medium

It is the nature of hadronic axions that they couple primarily to nuclear matter. Therefore, suitable astrophysical objects for investigating their properties are those which consist mainly of nucleons, e.g. supernovae, neutron stars, and accretion discs. The impact of axions on SN 1987A was already discussed in Chapter 3, while consequences of hadronic axions for neutron star and accretion disc physics will be explored in Chapter 6. The extent to which these objects are affected by axions depends strongly on the axion's emission and absorption properties. Therefore, we devote the present chapter to the axion emission rates and mean free path in neutron stars and accretion discs.

5.1 Axion Emission in a Nuclear Medium

5.1.1 Nucleon-Nucleon Axion Bremsstrahlung

As a consequence of the axion-nucleon coupling, axions can be produced in a nuclear medium via the nucleon-nucleon axion bremsstrahlung process $N + N \rightarrow N + N + a$, where N can be a proton p or a neutron n. For this production mechanism to be possible, one has to employ a spin-dependent nucleon-nucleon potential. An appropriate ansatz is the one-pion exchange (OPE) potential, which allows a simple calculation of the bremsstrahlung process. It should be stressed that using an OPE potential is just an approximation to the real nucleon interactions in hot and dense matter. However, since our goal is a simple estimate of the axion's influence on accretion discs and neutron stars, the OPE potential is a suitable assumption. Furthermore, we assume nonrelativistic nucleons. This is

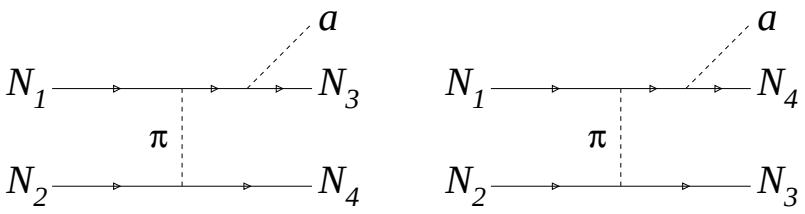

Figure 5.1: One possible Feynman diagram and its exchange graph for nucleon-nucleon axion bremsstrahlung. Altogether there are eight graphs, four direct and four exchange diagrams.

justified because the temperatures in neutron stars and accretion discs are around 100 keV and 10 MeV, respectively.

In the OPE approximation one has in total eight Feynman diagrams for the bremsstrahlung process: four direct diagrams with the axion attached to each nucleon line, and four exchange graphs each with $N_3 \leftrightarrow N_4$ (Fig. 5.1). For the "pure" processes $nn \to nn + a$ and $pp \to pp + a$ with only neutrons and protons, respectively, the spin-summed squared matrix element is found to be [33]

$$\sum_s |\mathcal{M}|^2_{NN} = \frac{256\pi^2\alpha_\pi^2}{3m_N^2}\, g_{aN}^2 \Bigg[\left(\frac{\mathbf{k}^2}{\mathbf{k}^2+m_\pi^2}\right)^2 + \left(\frac{\mathbf{l}^2}{\mathbf{l}^2+m_\pi^2}\right)^2 + \frac{\mathbf{k}^2\,\mathbf{l}^2 - 3(\mathbf{k}\cdot\mathbf{l})^2}{(\mathbf{k}^2+m_\pi^2)(\mathbf{l}^2+m_\pi^2)}\Bigg], \tag{5.1}$$

where $g_{aN} = C_N\, m_N/f_a$, $N = p, n$ is the axion-nucleon coupling constant and $\alpha_\pi = (f 2m_N/m_\pi)^2/4\pi$ the pion-nucleon "fine-structure constant" with the pion-nucleon coupling $f \simeq 1.05$. Furthermore, we have $\mathbf{k} = \mathbf{p}_2 - \mathbf{p}_4$ and $\mathbf{l} = \mathbf{p}_2 - \mathbf{p}_3$ with the nucleon's momenta $\mathbf{p}_i$. For the "mixed" process $np \to np + a$ one obtains

$$\begin{aligned}\sum_s |\mathcal{M}|^2_{np} \;=\; & \frac{256\pi^2\alpha_\pi^2}{3m_N^2}\,\frac{(g_{an}+g_{ap})^2}{4}\left[2\left(\frac{\mathbf{l}^2}{\mathbf{l}^2+m_\pi^2}\right)^2 - \frac{4\,(\mathbf{k}\cdot\mathbf{l})^2}{(\mathbf{k}^2+m_\pi^2)(\mathbf{l}^2+m_\pi^2)}\right] \\ & + \frac{256\pi^2\alpha_\pi^2}{3m_N^2}\,\frac{g_{an}^2+g_{ap}^2}{2}\Bigg[\left(\frac{\mathbf{k}^2}{\mathbf{k}^2+m_\pi^2}\right)^2 + 2\left(\frac{\mathbf{l}^2}{\mathbf{l}^2+m_\pi^2}\right)^2 \\ & + 2\frac{\mathbf{k}^2\,\mathbf{l}^2 - (\mathbf{k}\cdot\mathbf{l})^2}{(\mathbf{k}^2+m_\pi^2)(\mathbf{l}^2+m_\pi^2)}\Bigg].\end{aligned} \tag{5.2}$$

The larger coefficients compared to (5.1) are a consequence of the stronger couplings of charged pions to nucleons. To obtain the axion energy loss rate per unit

volume, one has to perform the phase-space integration

$$Q_a = \int \prod_{j=1}^{4,a} \frac{d^3p_j}{2E_j(2\pi)^3} E_a\, S \sum_s |\mathcal{M}|^2\, f_1 f_2 (1-f_3)(1-f_4) \\ \times\, (2\pi)^4\, \delta^{(4)}(P_1 + P_2 - P_3 - P_4 - P_a), \tag{5.3}$$

where P_j, $j = 1, \ldots, 4$ are the four-momenta of the external nucleons, P_a the one of the axion, and f_j, $j = 1, \ldots, 4$ the phase-space distributions of the nucleons. The factor S takes identical particles in the initial and final states into account: $S = 1/4$ for the pure, and $S = 1$ for the mixed processes. The Bose stimulation factor for the final-state axion $(1 + f_a)$ was neglected because we will see that these particles always escape freely.

To be able to perform the phase-space integration one needs to specify the phase-space distributions f_i of the nucleons. For accretion discs and neutron stars this is a difficult task. Therefore, as a first approximation we describe the nuclear medium in these objects as an ideal gas of protons, neutrons, and electrons, where neutrons and protons have approximately the same mass of $m_N \approx 940$ MeV. Then, the phase-space occupation function of protons ($i = p$) and neutrons ($i = n$) is given by the Fermi-Dirac distribution

$$f(\mathbf{p}_i) = \frac{1}{\exp[(E_i(\mathbf{p}_i) - \mu_i)/T] + 1}\,. \tag{5.4}$$

As the nucleons are nonrelativistic, it is appropriate to use the nonrelativistic kinetic energies $E_i^{\rm kin} = E_i(\mathbf{p}_i) - m_i \approx \mathbf{p}_i^2/2\,m_i$ and the nonrelativistic chemical potentials $\hat{\mu}_i = \mu_i - m_i$.

The integration in (5.3) simplifies considerably for degenerate or nondegenerate conditions, limits which pertain to neutron stars and accretion discs, respectively. For the latter, characteristic temperatures and densities are around $T \lesssim 10$ MeV and $\rho_B \approx 10^{12}$ g cm^{-3}, respectively, so that we find for the nucleon (nonrelativistic) Fermi energy

$$\varepsilon_{F,N} = p_{F,N}^2/2\,m_N = (3\pi^2 Y_N n_B)^{2/3}/2\,m_N \approx 1 \times Y_N^{2/3}\ {\rm MeV} \ll T, \tag{5.5}$$

where $n_B = N_B/V$ is the baryon number density and $Y_N = N_N/N_B$ with $N = n$ or p the nucleon number fraction. We see that neutrons and protons are nondegenerate. In the case of neutron stars, we have $T = 100$ keV and $\rho_B \approx 2\rho_{\rm nuc} \approx 5.6 \times 10^{14}$ g cm^{-3}, where $\rho_{\rm nuc} = 2.8 \times \times 10^{14}$ g cm^{-3} is the nuclear

density. In Appendix B we will show that the proton number fraction Y_p is around 0.01 so that

$$\varepsilon_{F,n} \approx 94 \text{ MeV} \gg T, \qquad \varepsilon_{F,p} \approx 4 \text{ MeV} \gg T, \tag{5.6}$$

i.e. both neutrons and protons are degenerate.

5.1.2 Nondegenerate Limit

For a nondegenerate nucleon gas the phase space integration (5.3) can not be done analytically. To simplify the squared matrix elements (5.1) and (5.2), we first neglect the pion mass m_π in the pion propagator. One then obtains

$$\sum_s |\mathcal{M}|^2_{NN} = \frac{256\pi^2\alpha_\pi^2}{3m_N^2}\,\tilde{g}^2_{NN} \tag{5.7}$$

with

$$\tilde{g}^2_{NN} \equiv \begin{cases} g_{an}^2\,(3-\beta) & nn \to nn + a \\ g_{ap}^2\,(3-\beta) & pp \to pp + a \\ \left(\dfrac{g_{an}+g_{ap}}{2}\right)^2 (2-4\beta/3) + \left(\dfrac{g_{an}^2+g_{ap}^2}{2}\right)(5-2\beta/3) & np \to np + a\,. \end{cases}$$

Here, $\tilde{g}_{NN} = \tilde{C}_N m_N/f_a$ is an effective coupling and $\beta \equiv 3\langle(\hat{\mathbf{k}}\cdot\hat{\mathbf{l}})^2\rangle$. In the nondegenerate limit it turns out that $\beta = 1.3078$ [34]. Numerically, one finds with the axion-nucleon couplings of expression (2.50)

$$|\tilde{C}_N| = \begin{cases} 0.013 & nn \to nn + a \\ 0.442 & pp \to pp + a \\ 0.495 & np \to np + a\,. \end{cases} \tag{5.8}$$

However, neglecting the pion mass will not be appropriate if one considers accretion discs: in a nondegenerate thermal medium of nonrelativistic nucleons with temperature T, the momenta of the nucleons are approximately given through $\mathbf{p}_i^2 \approx 3m_N T$. Since the temperatures in accretion discs are $T \approx 10$ MeV or below, typical nucleon momenta are $|\mathbf{p}_i| \approx 170$ MeV, comparable to the pion mass $m_\pi = 135$ MeV. Hence, in accretion discs one expects the pion masses to affect the axion emission rates so that we introduce the "fudge factor" $\xi(T)$ which includes all pion-mass effects. A rough estimate of $\xi(T)$ in Appendix A yields approximately 0.5. With a constant matrix element it is then straightforward to

perform the integration in expression (5.3). One obtains for the total energy loss rate per unit volume

$$\begin{aligned} Q_a^{\rm ND} &= \frac{\xi(T)}{280}\frac{T^{7/2}\,n_B^2}{m_N^{5/2}\pi^{7/2}}\left(Y_n^2\sum_s|\mathcal{M}|^2_{nn}+Y_p^2\sum_s|\mathcal{M}|^2_{pp}+4\,Y_nY_p\sum_s|\mathcal{M}|^2_{np}\right)\\ &= \frac{32}{105}\xi(T)\frac{\alpha_\pi^2\,T^{7/2}\,n_B^2}{m_N^{9/2}\pi^{3/2}}\left(Y_n^2\,\tilde{g}^2_{nn}+Y_p^2\,\tilde{g}^2_{pp}+4\,Y_nY_p\,\tilde{g}^2_{np}\right)\\ &\equiv \frac{32}{105}\xi(T)\frac{\alpha_\pi^2\,T^{7/2}\,n_B^2}{m_N^{9/2}\pi^{3/2}}g^2_{\rm ND}\,, \end{aligned} \tag{5.9}$$

where $g_{\rm ND}$ is the total effective axion-nucleon coupling constant for the nondegenerate limit. With $Y_p\approx 0.1$, $Y_n\approx 0.9$, and (5.8) we find numerically

$$g_{\rm ND}=4.71\times10^{-8}\,m_a \qquad \text{or} \qquad C_N^{\rm ND}=0.30\,. \tag{5.10}$$

Finally, we arrive at an axion energy loss rate per unit volume of

$$Q_a^{\rm ND}=4.89\times10^{27}\,{\rm erg\,cm^{-3}s^{-1}}\,T^{3.5}_{\rm MeV}\,\rho_{12}^2\,m^2_{\rm eV} \tag{5.11}$$

and at

$$L_a^{\rm ND}=9.7\times10^{48}\,{\rm erg\ s^{-1}}\,T^{3.5}_{\rm MeV}\,\rho_{12}\,\left(\frac{M}{M_\odot}\right)m^2_{\rm eV}. \tag{5.12}$$

for the total axion luminosity. $M_\odot$ is the solar mass and M the one of the accretion torus.

5.1.3 Degenerate Limit

In the degenerate limit, the parameter β is zero so that we obtain from (5.7) the squared matrix elements

$$\sum_s|\mathcal{M}|^2_{NN}=\frac{256\pi^2\alpha_\pi^2}{m_N^2}\,\tilde{g}^2_{NN} \tag{5.13}$$

with

$$\tilde{g}^2_{NN}=\begin{cases} g_{an}^2 & nn\to nn+a\\ g_{ap}^2 & pp\to pp+a\\ g_{an}^2+g_{ap}^2+g_{ap}^2g_{ap}^2/3 & np\to np+a\,. \end{cases}$$

Numerically, the effective coupling is

$$|\tilde{C}_N|=\begin{cases} 0.01 & nn\to nn+a\\ 0.34 & pp\to pp+a\\ 0.338 & np\to np+a\,. \end{cases} \tag{5.14}$$

With these matrix elements one can determine the axion volume emission rate. In the degenerate limit, there is no need for introducing a fudge factor $\xi(T)$ because the integration in (5.3) can be performed analytically without neglecting the pion masses. It turns out that the $m_\pi = 0$ rates must be supplemented with a factor [17]

$$F(u) = 1 - \frac{5u}{6}\arctan\left(\frac{2}{u}\right) + \frac{u^2}{3(u^2+4)} + \frac{u^2}{6\sqrt{2u^2+4}} \times \arctan\left(\frac{2\sqrt{2u^2+4}}{u^2}\right), \tag{5.15}$$

where $u \equiv m_\pi/p_{F,N}$. For a neutron star with $\rho_B \approx 2\rho_{\rm nuc}$, one has $u \approx 0.32\, Y_N^{-1/3}$ so that we may write $F(Y_N)$. Finally, we find for the total emission rate [17]

$$\begin{aligned} Q_a^{\rm D} &= \frac{31}{967680}\left(\frac{3\,n_B}{\pi}\right)^{1/3} T^6 \left(Y_n^{1/3}\, F(Y_n) \sum_s |\mathcal{M}|^2_{nn} + Y_p^{1/3}\, F(Y_p) \sum_s |\mathcal{M}|^2_{pp} \right. \\ &\qquad \left. + 4\, Y_{np}^{1/3}\, F(Y_{np}) \sum_s |\mathcal{M}|^2_{np} \right) \\ &= \frac{31\pi^{5/3}(3n_B)^{1/3}\alpha_\pi^2\, T^6}{3780\, m_N^2} \left(Y_n^{1/3}\, F(Y_n)\, \tilde{g}_{an}^2 + Y_p^{1/3}\, F(Y_p)\, \tilde{g}_{ap}^2 + Y_{np}^{1/3}\, F(Y_{np})\, \tilde{g}_{np}^2 \right) \\ &\equiv \frac{31\pi^{5/3}(3n_B)^{1/3}\alpha_\pi^2\, T^6}{3780\, m_N^2}\, g_{\rm D}^2\,, \end{aligned} \tag{5.16}$$

where $g_{\rm D}$ is the total effective axion-nucleon coupling constant for the degenerate limit and Y_{np} the effective nucleon fraction for the mixed processes. According to Brinkmann and Turner [33], the latter is given by

$$Y_{np}^{1/3} = \frac{1}{2\sqrt{2}}\left(Y_n^{2/3} + Y_p^{2/3}\right)^{1/2} \left[2 - \frac{|Y_n^{2/3} - Y_p^{2/3}|}{Y_n^{2/3} + Y_p^{2/3}}\right]. \tag{5.17}$$

With $Y_p = 0.01$ and $Y_n = 0.99$ one has $Y_{np} = 0.06$, and we can determine the suppression due to non-vanishing pion masses for the nn-, pp-, and np-processes, $F(Y_n) \approx 0.64$, $F(Y_p) \approx 0.12$, and $F(Y_{np}) \approx 0.31$. Altogether, we arrive at the following effective coupling constant

$$g_{\rm D} = 2.04 \times 10^{-8}\, m_a \qquad \text{or} \qquad C_N^{\rm D} = 0.13\,. \tag{5.18}$$

This together with (5.16) leads to the following expressions for the axion emission rate per unit volume,

$$Q_a^{\rm D} = 3.74 \times 10^{29}\ {\rm erg\ cm^{-3}\ sec^{-1}}\ T_{\rm MeV}^6\, m_{\rm eV}^2 \left(\frac{\rho_{\rm NS}}{\rho_{\rm nuc}}\right)^{1/3}, \tag{5.19}$$

where $m_{\rm eV} \equiv m_a/{\rm eV}$ and $T_{\rm MeV} \equiv T/{\rm MeV}$. Finally, we calculate the total axion luminosity $L_a^{\rm D}$ and obtain

$$L_a^{\rm D} = 3.4 \times 10^{49}\ {\rm erg\ yr^{-1}}\, m_{\rm eV}^2 \left(\frac{M}{M_\odot}\right) \left(\frac{\rho_{\rm NS}}{\rho_{\rm nuc}}\right)^{-2/3} T_9^6\ , \tag{5.20}$$

where M is the mass of the neutron star and $T_9 \equiv T/10^9\,{\rm K}$.

5.2 Axion Absorption in a Nuclear Medium

The energy loss of a star due to particle emission depends on whether these particles are trapped or not. In this section we will show that axions stream away freely both from neutron stars and accretion discs.

The dominant absorption process for axions is inverse axion bremsstrahlung $N + N + a \to N + N$. The associated mean free path λ_a of the axion is related to its absorption rate $\Gamma_{\rm abs}$ through $\lambda_a^{-1} = \Gamma_{\rm abs}$. One obtains

$$\begin{aligned} \lambda_a^{-1} = \Gamma_{\rm abs} \ &= \ e^{E_a/T} \int \prod_{j=1}^{4} \frac{d^3p_j}{2E_j(2\pi)^3} \left(\frac{1}{2E_a}\right) S \sum_s |\mathcal{M}|^2\, f_1 f_2 (1-f_3)(1-f_4) \\ &\quad \times (2\pi)^4\, \delta^{(4)}(P_1 + P_2 - P_3 - P_4 - P_a), \end{aligned} \tag{5.21}$$

where E_a is the axion energy. The factor $e^{E_a/T}$ accounts for the detailed-balance relationship which reveals that $\Gamma_{\rm em} = \exp(-E_a/T)\,\Gamma_{\rm abs}$, where $\Gamma_{\rm em}$ is the axion emission rate. A comparison between (5.3) and (5.21) shows that the volume emission rate Q_a is related to the mean free path by

$$Q_a = \frac{1}{(2\pi)^3} \int_0^\infty \lambda_a^{-1} e^{-E_a/T} E_a\, dp_a^3\,. \tag{5.22}$$

In the case of the nondegenerate limit, one obtains for the axion's inverse mean free path [17]

$$\lambda_a^{{\rm ND}\,-1} = \frac{\xi(T)\pi^{1/2}\alpha_\pi^2\, n_B^2}{6\, m_N^{9/2}\, T^{1/2}} \frac{\sqrt{1 + x\pi/4}}{x}\, g_{\rm ND}^2\,, \tag{5.23}$$

where $x \equiv E_a/T$. For freely streaming axions, the average energy is determined by the nondegenerate nucleon-nucleon bremsstrahlung axion spectrum. We find $\langle x \rangle = \langle E_a \rangle / T = 16/7$ so that

$$\lambda_a^{{\rm ND}\,-1} = 3.09 \times 10^{-9}\ {\rm cm^{-1}}\, T_{\rm MeV}^{-0.5}\, \rho_{12}^2\, m_{\rm eV}^2 \tag{5.24}$$

or

$$\lambda_a^{\rm ND} \approx 3240 \text{ km } T_{\rm MeV}^{0.5}\, \rho_{12}^{-2}\, m_{\rm eV}^{-2}. \tag{5.25}$$

In accretion discs, the maximum temperatures and densities are 10 MeV and 10^{12} g cm^{-3}, respectively. Then, one obtains for the mean free path of an 20 eV axion $\lambda_a \approx 26$ km. The maximum geometrical dimensions of accretion discs are about 50 km so that it is not clear if axions escape freely. However, as we have used extreme vales for T and ρ, the average mean free path will be larger than 26 km so that freely streaming axions are a good approximation.

In the degenerate case, the inverse mean free path is given by [17]

$$\lambda_a^{\rm D\,-1} = \frac{(3n_B)^{1/3}\alpha_\pi^2\, T^2}{24\pi^{7/3} m_N^2} \frac{(x^2+4\pi^2)}{(1-e^{-x})}\, g_{\rm D}^2 \tag{5.26}$$

or numerically,

$$\lambda_a^{\rm D} \approx 8350 \text{ km } m_{\rm eV}^{-2}\, T_9^{-2} \left(\frac{\rho_{\rm NS}}{\rho_{\rm nuc}}\right)^{-1/3}, \tag{5.27}$$

where we have used the average axion energy $\langle x\rangle = \langle E_a\rangle/T \approx 3.16$, which can be calculated using the degenerate nucleon-nucleon bremsstrahlung axion spectrum [17]. For a neutron star with $T \approx 10^9$ K and $\rho \approx 2\rho_{\rm nuc}$ we obtain

$$\lambda_a^{\rm D} \approx 6630 \text{ km } m_{\rm eV}^{-2}\,. \tag{5.28}$$

Axions of mass m_a are not trapped inside a neutron star of radius R if $\lambda_a \gtrsim R$. For $R \approx 10$ km this is fulfilled for

$$m_a \lesssim 26 \text{ eV}\,. \tag{5.29}$$

Therefore, axions in the hadronic axion window are allowed to stream freely from neutron star interiors. As we will discuss more precisely in Chapter 3, one expects parts of the neutron-star matter to be in a superfluid state. If so, the mean free path (5.28) is significantly enhanced.

Chapter 6

Impact on Black Hole Accretion Discs and Neutron Stars

We explore how the emission of axions with parameters in the hadronic axion window affects the evolution of gamma-ray bursts. We assume that a subclass of short bursts with a duration of 0.1–1 seconds is driven by the accretion of hot plasma by a black hole. Axion production in this accretion torus would provide a significant energy loss, altering the final γ-fluence. Moreover, we investigate the impact of an hadronic-axion energy loss on the cooling timescale of neutron stars. We find a relation between their present surface temperature and the axion mass. Our results are then compared with the observational data of the pulsars PSR 1055-52, PSR 0630+178 (Gemina), and PSR 0656+14. Finally, we discuss effects of nucleon superfluidity on our calculation.

6.1 Gamma-Ray Bursts

6.1.1 General Picture

Gamma-ray bursts are short and intense bursts of photons with energies in the range between approximately 100 keV and 1 MeV. In fact, gamma-ray bursts are the electromagnetically most luminous objects observed in the universe. Since their discovery in the late sixties, several satellites have observed them, and numerous theories have been developed to explain their physical nature. A milestone in the exploration of gamma-ray bursts was a remarkable finding of the BATSE detector, which was launched in the spring of of 1991. BATSE measured a per-

fectly isotropic angular distribution of gamma-ray bursts and a deficiency of faint bursts [35]. This led to the suggestion that gamma-ray bursts are cosmological, an assumption that was confirmed by the discovery of x-ray transient counterparts by Beppo-SAX [36], and later by the discovery of optical [37] and radio counterparts [38]. For the first time, it was possible to rule out a wide class of gamma-ray burst theories!

In spite of these discoveries, the origin of gamma-ray bursts remains unclear. However, there exists a promising generic model which is in agreement with observation: the "fireball model," where an ultra-relativistic energy flow is converted into radiation. The initial energy flow can be an electromagnetic Pointing flux or kinetic energy of highly-relativistic particles. As the conversion in radiation takes place in an optically thin region, gamma-ray burst spectra are nonthermal, in agreement with observation.

6.1.2 The BHAD Model

The nature of the central engine that drives the gamma-ray burst remains unclear because the "inner engine" that powers the relativistic fireball is hidden from direct observations. While many models have been proposed, those currently favored are all based on the rapid accretion of matter by a black hole. These models are referred to as black hole accretion disk (BHAD) models. It must be stressed that BHAD models are only able to explain short gamma-ray bursts with durations in the range 0.1–1 s. Several promising candidates for the progenitor system of a BHAD have been proposed, the most popular being neutron star binaries, which we presently focus on.

The merger of two neutron stars leads to a hot and dense central object with masses around 3 $M_\odot$, surrounded by a toroidal cloud of hot plasma gas with a mass of about 0.1–0.2 $M_\odot$. Within a timescale of a few milliseconds, the 3 $M_\odot$ core will most likely collapse to a black hole. However, a significant amount of mass, typically 0.03–0.3 $M_\odot$, has too much angular momentum to be swallowed immediately by the black hole, and an accretion disc forms. Such accretion discs have masses between several 10^{-2} $M_\odot$ and a few 10^{-1} $M_\odot$. Their densities are around 10^{10}–10^{12} g cm^{-3}, their temperatures in the range between 3 and 10 MeV.

Within this accretion torus neutrinos of all flavors are produced by different processes. The bulk of the neutrino luminosity is provided by the electron neutrinos ν_e and $\bar{\nu}_e$, which are mainly produced by the charged-current processes of

electron and positron capture on protons and neutrons [39],

$$\begin{aligned} e^- + p &\longrightarrow n + \nu_e \,, \\ e^+ + n &\longrightarrow p + \bar{\nu}_e \,. \end{aligned} \tag{6.1}$$

Second is the muon and tau neutrino production, principally via electron-positron pair annihilation

$$e^- + e^+ \longrightarrow \nu_i + \bar{\nu}_i \,, \qquad i = \mu \text{ or } \tau \,. \tag{6.2}$$

Depending on the specific BHAD model, electron neutrinos are emitted from a neutrinosphere with an outer radius of 70–100 km. Moreover, muon and tau neutrinos may be trapped, depending on the thermodynamic properties of the torus [7]. The total neutrino luminosities L_ν are typically in the ballpark of 10^{53} erg s^{-1}.

Now we come to the crucial point concerning gamma-ray bursts. The emitted neutrinos and antineutrinos interact with each other and annihilate into electron-positron pairs. The efficiency of this energy deposition $E_{\nu\bar{\nu}}$ in form of an electron-positron plasma is usually expressed in terms of the parameter $q_{\nu\bar{\nu}} \equiv \dot{E}_{\nu\bar{\nu}}/L_\nu$, where $\dot{E}_{\nu\bar{\nu}}$ is the rate of energy deposition by neutrino-antineutrino annihilation. The efficiency $q_{\nu\bar{\nu}}$ depends on the number densities and energies of the initial neutrinos. According to [7], typical values for $q_{\nu\bar{\nu}}$ are around 0.004, i.e. only a half percent of the initial neutrino energy is transformed into thermal energy of an electron-positron plasma, the fireball. Integrated over the accretion timescale $\tau \approx$ 5–50 ms, the total energy deposition is of order 10^{49} erg. Moreover, it is possible that the fireball does not expand isotropically, but is beamed into axial jets with a fraction $f_\Omega = 2\delta\Omega/4\pi$ of the whole sky. Including a beaming factor $f_\Omega \approx 0.1$–0.01, it follows that the BHAD scenario is able to account for short gamma-ray bursts with energies in the range of 10^{50}–10^{51} erg.

6.1.3 Influence of Hadronic Axion Emission

Let us now examine to what extent hadronic axions could alter the BHAD model for gamma-ray bursts. During the process of accretion, axions could be produced by nucleon-nucleon axion bremsstrahlung. Clearly, in order to maintain the BHAD model, the total axion luminosity L_a may not exceed the neutrino luminosity L_ν, which is of about 10^{53} erg s^{-1}.

We consider two BHAD models that have been investigated in great detail [7]. The first describes the attractive force of the central black hole by a Newtonian

Table 6.1: Temperature T, density ρ, mass M and neutrino luminosity L_ν of an accretion disc for the Newtonian and the Paczyński-Wiita model. $\overline{T}$, $\overline{\rho}$, $\overline{M}$, and $\overline{L}_\nu$ are the associated averaged quantities.

	Newtonian model	Paczyński-Wiita model
T [MeV]	2–10	2–10
$\overline{T}$	6	4
ρ [10^{12} g cm^{-3}]	0.01–1	0.01–0.3
$\overline{\rho}$	0.3	0.1
M [$M_\odot$]	0.16–0.29	0.002–0.031
$\overline{M}$	0.23	0.02
L_ν [10^{52} erg s^{-1}]	1–12	0.14–6.7
$\overline{L}_\nu$	5.6	4.4

gravitational potential, which is known to be singular at the origin $r = 0$. The second takes general-relativistic effects into account by allowing one to reproduce the existence of a last stable circular orbit at a radius of $3r_s = 6GM_{\rm BH}/c^2$, where r_s is the Schwarzschild radius. This model is referred to as the Paczyński-Wiita model. The resulting temperatures T, densities ρ, and accretion disc masses M for both models are shown in Tab. 6.1 as well as the mean values of these quantities. One sees that the torus masses in the Paczyński-Wiita model are much smaller than those of the Newtonian model. This is a result of the very strong gravitational potential of the Paczyński-Wiita model, implying that the accretion rates, i.e. the mass accretion into the black hole per unit time, of this model are much greater than those in the Newtonian description. Therefore, the torus mass of the latter is significantly higher than the one of the former model. However, it might be that the Paczyński-Wiita model underestimates the torus mass.

Now, we want to estimate the axion luminosity L_a. As we have seen in the previous chapter, axions stream away freely from accretion discs, implying that axion volume emission takes place. The corresponding energy loss is given by expression (5.12). It is linear in the mass M and the density ρ so that one may use the average values given in Tab. 6.1. Then, one finds for the two models

$$L_a = \begin{cases} 6.7 \times 10^{47}\ \text{erg s}^{-1}\, T_{\rm MeV}^{3.5}\, m_{\rm eV}^2 & \text{Newtonian model} \\ 1.9 \times 10^{46}\ \text{erg s}^{-1}\, T_{\rm MeV}^{3.5}\, m_{\rm eV}^2 & \text{Paczyński-Wiita model.} \end{cases} \tag{6.3}$$

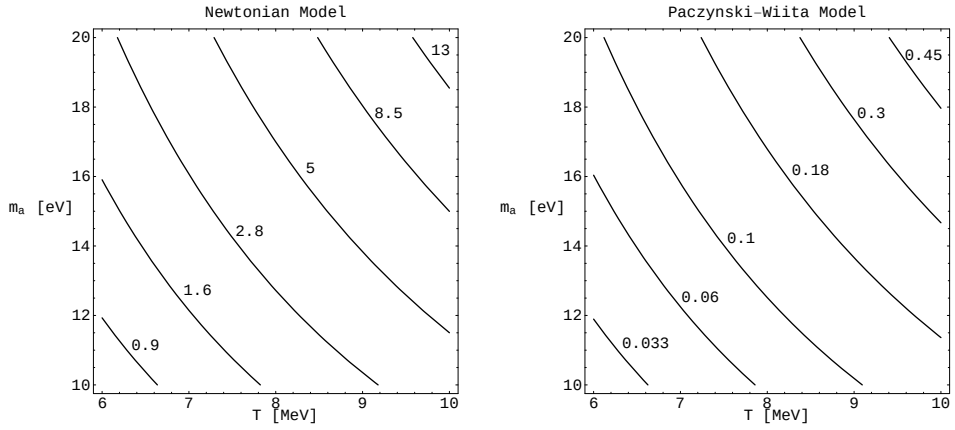

Figure 6.1: Axion luminosity relative to the one of neutrinos $L_a/\overline{L}_\nu$ as a function of the temperature T and the axion mass m_a. The left and right panels are based on the Newtonian and Paczyński-Wiita model, respectively.

Now, these luminosities have to be compared with those of the neutrinos given in Tab. 6.1. This is graphically done in Fig. 6.1, where the ratio $L_a/\overline{L}_\nu$ as a function of the temperature T and the axion mass m_a is plotted.

Obviously, in the case of the Newtonian model, hadronic axions could alter the existence of gamma-ray bursts, whereas for the Paczyński-Wiita model the axion luminosities are at least one order of magnitude smaller than the one of the neutrinos. This is a consequence of the small torus masses in the Paczyński-Wiita model.

Finally, we want to estimate the maximum axion production rate which can be obtained for the maximum temperature $T \approx 10$ MeV. With (6.3) we find

$$L_a = \begin{cases} 2.1 \times 10^{51}\ \mathrm{erg\ s^{-1}}\, m_{\mathrm{eV}}^2 & \text{Newtonian model} \\ 6.0 \times 10^{49}\ \mathrm{erg\ s^{-1}}\, m_{\mathrm{eV}}^2 & \text{Paczyński-Wiita model.} \end{cases} \tag{6.4}$$

As a result, one obtains an upper bound on the allowed axion mass of approximately

$$m_a \lesssim \begin{cases} 5\ \mathrm{eV} & \text{Newtonian model} \\ 27\ \mathrm{eV} & \text{Paczyński-Wiita model.} \end{cases} \tag{6.5}$$

It is not clear which of both models gives an appropriate description of the accretion process, or whether they are a good approximation of the black hole gravitational potential at all. Therefore, we estimate that axions in the parameter

range between 10 and 100 eV are in principle able to alter the evolution of gamma-ray bursts significantly. Note that this range includes the hadronic axion window of 10–20 eV, i.e. the existence of hadronic axions would be relevant for gamma-ray burst physics.

Presently, nobody knows whether the BHAD model gives the correct description of gamma-ray bursts. However, if this picture proves to be correct, at least for short gamma-ray bursts, one could calculate reliable bounds on the axion mass. On the other hand, if hadronic axions were detected by the solar-axion search experiments [40, 41], the BHAD model certainly would have to include axion emission in a detailed description.

6.2 Neutron Stars

6.2.1 A Simple Model for Axion Cooling

We showed in the Sect. 5.2 that axions in the hadronic axion window are allowed to stream freely from neutron star interiors, implying an additional energy loss which could have observable consequences which shall now be explored. Therefore, we set up a simple model of late-time neutron star cooling, assuming that the star cools via axion volume emission. Furthermore, we neglect all other cooling mechanisms because axions only alter neutron star cooling significantly if they are the dominant cooling channel. The corresponding axion luminosity was given in (5.20),

$$L_a = 3.4 \times 10^{49}\ \text{erg yr}^{-1}\, m_{\text{eV}}^2 \left(\frac{M}{M_\odot}\right) \left(\frac{\rho_{\text{NS}}}{\rho_{\text{nuc}}}\right)^{-2/3} T_9^6\ . \tag{6.6}$$

This result is based on the assumption that the nuclear medium can be treated as an ideal, degenerate Fermi gas of neutrons and protons. However, the real nuclear equation of state of the superdense matter inside a neutron star is still unknown. According to the BCS theory of superfluidity, one expects parts of the neutron star to be in a superfluid state. At lower densities $\rho \approx 10^{13}$–10^{14}g cm^{-3} particles are expected to be in a $^1\text{S}_0$ superfluid state when the temperature falls below the critical temperature T_{cr}. A second superfluid state $^3\text{P}_2$ occurs in more dense matter with $\rho \approx 10^{14}$–10^{15}g cm^{-3}, implying that neutrons in the core of neutron stars should be in this superfluid state. As the density of protons in a neutron star is much smaller than the one of the neutrons, they are expected to

be in the $^1S_0$ state. However, superfluidity in neutron stars is a difficult matter, and many of its aspects are not yet understood. Particularly controversial is the proton $^1S_0$ pairing. But, if superfluidity occurs, it has different effects on the cooling of neutron stars; the most important in the context with axion emission is the suppression of our estimated axion-nucleon interaction (5.18). Moreover, strong superfluidity reduces the heat capacity C of the nucleon gas. We include these effects by introducing an effective axion luminosity and heat capacity,

$$L_a^{\rm eff} = \frac{1}{f_{\rm em}}\, L_a \equiv \frac{1}{f_{\rm em}} A\, T_9^6 \qquad \text{and} \qquad C_{\rm eff} = \frac{1}{f_{\rm C}}\, C, \tag{6.7}$$

respectively, where $f_{\rm em}$ and f_C are fudge factors.

The effective axion luminosity is linked with an energy loss of the neutron star. According to our simple model of nuclear matter, the total, unsuppressed heat capacity C of a neutron star is that of a degenerate ideal gas of neutrons, protons, and electrons,

$$C = \frac{\pi^2}{2} T \left(\frac{N_n}{\varepsilon_{F,n}} + \frac{N_p}{\varepsilon_{F,p}} + \frac{N_e}{\varepsilon_{F,e}} \right), \tag{6.8}$$

where N_n, N_p, and N_e are the numbers of neutrons, protons, and electrons and $\varepsilon_{F,n}$, $\varepsilon_{F,p}$, and $\varepsilon_{F,ne}$ are the related Fermi energies. For nonrelativistic nucleons $i = n, p$ one has $p_{F,i} = (3\pi^2 Y_i\, n_B)^{1/3} \equiv p_{F,N} Y_i^{1/3}$ and $\varepsilon_{F,i} = p_{F,i}^2/2m_N \equiv \varepsilon_{F,N} Y_i^{2/3}$ whereas $\varepsilon_{F,e} = p_{F,e}$ for the relativistic electrons. Charge neutrality implies $n_e = n_p$ and thus $p_{F,e} = p_{F,p}$ so that $\varepsilon_{F,e} = p_{F,p}$. Finally we obtain

$$\begin{aligned} C &= \frac{\pi^2}{2} \frac{N_B T}{\varepsilon_{F,N}} \left(Y_n^{1/3} + Y_p^{1/3} + Y_p^{2/3}\, \frac{\varepsilon_{F,N}}{p_{F,N}} \right) \\ &= \frac{\pi^2}{2} \frac{N_B T}{\varepsilon_{F,N}} \left(0.997 + 0.215 + 0.009 \right), \end{aligned} \tag{6.9}$$

where we have used $Y_p = 0.01$. Obviously, neutrons, protons, and electrons contribute around 82%, 17% and 1%, respectively, to the total heat capacity C. If we express C in terms of the solar mass and the nuclear density, we find explicitly

$$C = 1.42 \times 10^{48} \frac{\rm erg}{10^9\ {\rm K}}\, T_9 \left(\frac{M}{M_\odot} \right) \left(\frac{\rho_{\rm NS}}{\rho_{\rm nuc}} \right)^{-2/3} \equiv B\, T_9. \tag{6.10}$$

As axions are considered to be the dominant cooling channel, one obtains as a result of energy conservation

$$\frac{dE_{\rm NS}}{dt} = C_{\rm eff}\, \frac{dT}{dt} = -L_a^{\rm eff}, \tag{6.11}$$

where $E_{\rm NS}$ is the total thermal energy of the neutron star. With (6.7) and (6.10) we obtain the equation

$$\frac{1}{f_C} B\, T_9\, \frac{dT_9}{dt} = -\frac{1}{f_{\rm em}} A\, T_9^6 \ . \tag{6.12}$$

This equation can be easily integrated with the result

$$\Delta t = t_f - t_i = \frac{B f_{\rm sup}}{4A}\, T_9(f)^{-4} \left(1 - \frac{T_9(f)^4}{T_9(i)^4}\right), \tag{6.13}$$

where $T_9(i) \equiv T_i/10^9$ K and $T_9(f) \equiv T_f/10^9$ K are the internal temperatures of the neutron star, taken at the initial and final times t_i and t_f, respectively. Furthermore, we have introduced the total fudge factor $f_{\rm sup} \equiv f_{\rm em}/f_C$. Without introducing any large errors, $T_9(f)/T_9(i)$ can be taken to be zero. Then (6.13) simplifies to

$$t_{\rm yr} \approx 0.010\, m_{\rm eV}^{-2}\, f_{\rm sup}\, T_9(f)^{-4} \tag{6.14}$$

or

$$T_{C9} = 0.32\, f_{\rm sup}^{1/4}\, m_{\rm eV}^{-1/2}\, t_{\rm yr}^{-1/4} \ , \tag{6.15}$$

where $t_{\rm yr} \equiv t_f/{\rm yr}$ is the neutron star age in years and $T_{C9} \equiv T_9(f)$. It should be stressed that T_{C9} is effectively the core temperature because we do not consider axion production in the neutron star crust. Consequently, equation (6.15) allows us to calculate the internal temperature T_C of a neutron star depending on its age $t_{\rm yr}$, the axion mass m_a, and the fudge factor $f_{\rm sup}$. A remarkable feature of the solution (6.15) is that it depends neither on the mass M nor on the density ρ of the neutron star.

In order to compare our prediction with observational data, it is appropriate to rewrite equation (6.15) in terms of the observable surface temperature T_S, instead of the internal temperature T_C. Strictly speaking, the temperature detected by a distant observer is not T_S, but the red-shifted temperature $T_S^\infty = T_S\sqrt{1 - R_g/R}$, where R_g is the gravitational radius. For neutron stars, the stellar radius R is only 2–3 times larger than R_g, i.e. $R/R_g = 2.5$. Therefore, we obtain the relation

$$T_S \approx 1.29\, T_S^\infty \ . \tag{6.16}$$

Furthermore, as a consequence of thermal conductivity, the core temperature T_C is related to the surface temperature T_S. Approximately, the following equation holds [42]:

$$T_{C9} = 0.128 \left(\frac{T_{S6}^4}{g_{14}}\right)^{5/11} \ , \tag{6.17}$$

Table 6.2: Measured effective surface temperatures $T^{\infty}_{S,\mathrm{obs}}$ and derived bounds on the ratio $f_{\mathrm{sup}}/m^2_{\mathrm{eV}}$, where f_{sup} is a fudge factor which takes the suppression of axion emission due to superfluidity into account.

Source	$\log t_{\mathrm{yr}}$	$\log T^{\infty}_{S,\mathrm{obs}}$ [K]	Exclusion range for $f_{\mathrm{sup}}/m^2_{\mathrm{eV}}$
PSR 1055-52	5.73	5.84–5.91	$f_{\mathrm{sup}}/m^2_{\mathrm{eV}} \lesssim 1167$
Gemina	5.53	5.67–5.80	$f_{\mathrm{sup}}/m^2_{\mathrm{eV}} \lesssim 43$
PSR 0656+14	5.00	5.93–5.98	$f_{\mathrm{sup}}/m^2_{\mathrm{eV}} \lesssim 975$

where $T_{S6} \equiv T_S/10^6$ K and g_{14} is the gravitational acceleration on the neutron star surface in units of 10^{14} cm sec^{-2}. Eliminating the temperature T_{C9} between the equations (6.15) and (6.17), leads together with (6.16) to

$$T^{\infty}_{S6} = 1.282\, g_{14}^{1/4}\, {f_{\mathrm{sup}}}^{11/80}\, m_{\mathrm{eV}}^{-11/40}\, t_{\mathrm{yr}}^{-11/80}\ . \tag{6.18}$$

The gravitational surface acceleration is typically in the range of $g_{14} \approx 2$–3. Therefore, with $g_{14} = 2.5$ and the logarithmic scales $\log T_S$ and $\log t_{\mathrm{yr}}$, we finally arrive at

$$\log T^{\infty}_S \approx 0.138\, \log\left(\frac{f_{\mathrm{sup}}}{m^2_{\mathrm{eV}}}\right) - 0.138\, \log t_{\mathrm{yr}} + 6.208, \tag{6.19}$$

where log is the logarithm to base 10. Now we are in a position to compare our predictions with the observational data from ROSAT. Axions with masses m_a are execluded if the predicted temperatures $\log T^{\infty}_S$ of expression (6.19) are below those observed, i.e. $T^{\infty}_S < T^{\infty}_{S,\mathrm{obs}}$. The measured effective surface temperatures $T^{\infty}_{S,\mathrm{obs}}$ and the ages of three pulsars PSR 1055-52 [43], PSR 0630+178 (Gemina) [44], and PSR 0656+14 [45] are listed in Tab. 6.2. Additionally, in the fourth column the exclusion ranges for $f_{\mathrm{sup}}/m^2_{\mathrm{eV}}$ are given for each source. To rule out the whole hadronic axion window between 10 and 20 eV, we obtain maximal allowed fudge factors f_{sup} of order 10^5, 4×10^3, and 10^5 for the pulsars PSR 1055-52, Gemina, and PSR 0656+14, respectively. Fig. 6.2 shows the predicted cooling curve of a neutron star according to our model. The axion mass is $m_a = 10$ eV and $m_a = 20$ eV for the dashed and solid curves, respectively. Furthermore, the fudge factor was supposed to be $f_{\mathrm{sup}} = 10^3$. In spite of this extreme suppression of the axion emission, the associated axion cooling predicts present-day surface temperatures $T^{\infty}_{S,\mathrm{obs}}$ which are far below the measured data, i.e. the observed neutron stars are too hot to have been cooled by hadronic axion emission.

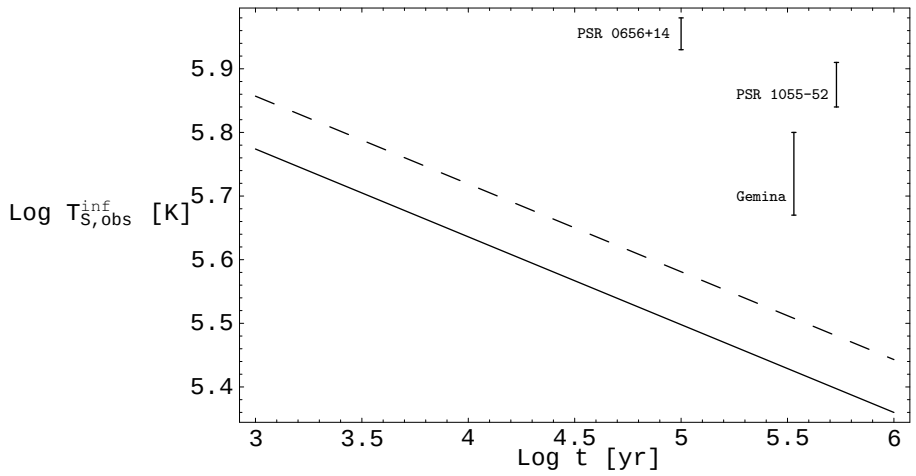

Figure 6.2: Red-shifted surface temperature $T^{\infty}_{S,\mathrm{obs}}$ versus age for axion cooling. The dashed and solid curves correspond to axion masses of 10 eV and 20 eV, respectively. The fudge factor f_{sup} was assumed to be 10^3.

6.2.2 Numerical Cooling Calculations Including Axions

Recently, Umeda et al. [8] have investigated the thermal evolution of neutron stars including axionic energy losses. They intended to compete with the low mass SN 1987A limit of equation (3.6), which implies the upper limit $m_a \lesssim 0.01$ eV on the axion mass. Just as we did above, they assumed axion emission due to nucleon-nucleon bremsstrahlung. They based their calculation on three equations of state, a stiff, a medium, and a soft one; corresponding to different compressibilities of the nuclear matter. Furthermore, they took $^3\mathrm{P}_2$ Cooper pairing of neutrons into account. Umeda et al. compared their results with the data of the PSR 0656+14 pulsar and obtained the limits

$$m_a \lesssim \begin{cases} 0.33 \text{ eV} & \text{stiff model} \\ 0.08 \text{ eV} & \text{medium model} \\ 0.06 \text{ eV} & \text{soft model,} \end{cases} \tag{6.20}$$

which are less stringent than the one of SN 1987A .

Nevertheless, we can gain from their calculation because it has implications for the hadronic axion window. Umeda et al. assumed that axions do not get trapped in the interior of neutron stars. Hence, their constraint applies as long as the free streaming condition $\lambda_a > R$ is satisfied. However, we have seen in

Sect. 5.2 that hadronic axions stream away freely, i.e. the result of Umeda et al. excludes axions with parameters of the hadronic axion window.

Over and above that, we can use their limits to estimate of the fudge factor $f_{\rm sup}$. With (6.20) and the condition $f_{\rm sup}/m_{\rm eV}^2 \gtrsim 975$ for the PSR 0656+14 we find

$$f_{\rm sup} \approx \begin{cases} 106 & \text{stiff model} \\ 6.2 & \text{medium model} \\ 3.5 & \text{soft model.} \end{cases} \tag{6.21}$$

The fudge factor $f_{\rm sup}$ is a compound parameter taking the suppression of axion emission and heat capacity due to superfluidity into account. In the case of the stiff equation of state, neutrons are assumed to be strongly superfluid, implying a significant reduction of their heat capacity—actually it becomes smaller than the one of the electrons so that neutrons effectively do not contribute to the total heat capacity C of the neutron star. We have seen above that neutrons contribute around 80% to the total heat capacity. Therefore, for the stiff model we estimate a heat-capacity fudge factor f_C of about 5, implying $f_{\rm em} \approx 530$. In models with a softer equation of state, the reduction of the heat capacity as a result of superfluidity is smaller, and the fudge factor is difficult to determine. Approximately, we use $f_C \approx 2$ and $f_C \approx 1$ for the medium and the soft model, respectively. Altogether we have

$$f_{\rm em} \approx \begin{cases} 530 & \text{stiff model} \\ 12 & \text{medium model} \\ 4 & \text{soft model} \end{cases} \tag{6.22}$$

for the suppression of the axion emission as a consequence of neutron superfluidity.

Now, we are in a position to specify the axion trapping inside a neutron star more precisely. The mean free path $\lambda_a^{\rm D}$ was given in equation (5.28), however, without taking superfluidity into account. The effective mean free path is given by $\lambda_a^{\rm eff} = f_{\rm em}\, \lambda_a^{\rm D}$, i.e.

$$\lambda_a^{\rm eff} \approx 6630 \text{ km } f_{\rm em}\, m_{\rm eV}^{-2}\,. \tag{6.23}$$

Axions get trapped if $\lambda_a^{\rm eff}$ is comparable to the neutron-star radius $R \approx 10$ km. Therefore, from (6.22) we obtain the following conditions for free streaming axions,

$$m_a \lesssim \begin{cases} 593 \text{ eV} & \text{stiff model} \\ 89 \text{ eV} & \text{medium model} \\ 51 \text{ eV} & \text{soft model.} \end{cases} \tag{6.24}$$

Hence, we conclude that axions do not get trapped in the interior of neutron stars if their masses are less than 50–600 eV.

6.3 Is the Hadronic Axion Window Closed?

We have re-examined the possibility of an astrophysically allowed KSVZ-type axion which has a strongly suppressed coupling to photons, and we have confirmed that such "hadronic axions" with masses between 10 and 20 eV are not excluded by previous arguments. Axions in this window were thermally produced in the early universe, implying that they constitute HDM with $\Omega_a \approx 0.1$–0.4, in agreement with the recent work of Moroi and Murayama [4]. Hence, hadronic axions not only solve the strong CP problem, but they are also of cosmological importance.

As hadronic axions mainly couple to nucleons, we have investigated their impact on accretion discs and isolated neutron stars. We have found that hadronic-axion production in accretion discs would have observable consequences if these objects really provide an explanation for short gamma-ray bursts as in the BHAD model. This model is based on coalescing compact binaries such as two neutron stars, implying the emission of gravitational waves which could in future be detected by the laser interferometers LIGO, VIRGO, TAMA, and GEO [46]. If so, a time-coincident observation of gamma-ray bursts and gravitational waves would be strong evidence for the BHAD model. However, even if the BHAD model proves to be true, it is premature to rule out hadronic axions because their emission rate from the accretion torus depends significantly on details of the BHAD model. On the other hand, a future detection of solar hadronic axions via resonant absorption in ^{57}Fe [40, 41] would have important consequences for the BHAD scenario, perhaps even calling this explanation for gamma-ray bursts into question.

The most significant limits on hadronic axions arise from old neutron stars. Our simple cooling model indicates that hadronic axions accelerate the cooling process of these objects significantly, with the consequence that neutron stars today are actually too hot to be in accord with hadronic axions. Even in the presence of superfluidity, which suppresses the emission rates, this discrepancy remains significant. The same conclusion is reached on the basis of the numerical neutron-star cooling simulations by Umeda et al. [8]. Conversely, if the existence of hadronic axions were verified, the standard cooling mechanism for neutron stars

would have a serious blemish. In this case, internal heating effects would have to be included [47] or the interpretation of the observed soft x-ray components of the pulsars PSR 1055-52, Gemina, and PSR 0656+14 [43, 44, 45] as thermal blackbody spectra would have to be reconsidered.

Appendix A

Pion Mass Effects in the Bremsstrahlung Process

It was mentioned in Chapter 5 that the influence of non-zero pion masses m_π on the axion emission via nucleon-nucleon axion bremsstrahlung is a temperature dependent effect, and that the necessary phase-space integrations can not be done analytically in the case of the nondegenerate limit. It is therefore appropriate to estimate these effects as a function of the temperature. Recall that the squared matrix element for nucleon-nucleon axion bremsstrahlung is

$$\sum_s |\mathcal{M}|^2 = \frac{256\pi^2}{3}\frac{g_{aN}^2\alpha_\pi^2}{m_N^2}\left[\left(\frac{\mathbf{k}^2}{\mathbf{k}^2+m_\pi^2}\right)^2+\left(\frac{\mathbf{l}^2}{\mathbf{l}^2+m_\pi^2}\right)^2 + \frac{\mathbf{k}^2\,\mathbf{l}^2-3(\mathbf{k}\cdot\mathbf{l})^2}{(\mathbf{k}^2+m_\pi^2)(\mathbf{l}^2+m_\pi^2)}\right], \tag{A.1}$$

where $\mathbf{k}=\mathbf{p}_2-\mathbf{p}_4$ and $\mathbf{l}=\mathbf{p}_2-\mathbf{p}_3$ with the nucleon's momenta $\mathbf{p}_i,\ i=1\ldots4$. For zero pion masses (A.1) becomes

$$\sum_s |\mathcal{M}|^2\bigg|_{m_\pi=0} = \frac{256\pi^2}{3}\frac{g_{aN}^2\alpha_\pi^2}{m_N^2}(3-\beta) \tag{A.2}$$

with $\beta \equiv 3\langle(\hat{\mathbf{k}}\cdot\hat{\mathbf{l}})^2\rangle = 1.3078$.

In a thermal medium the momenta of nonrelativistic nucleons are on average $\langle\mathbf{p}^2\rangle \approx 3m_NT$, so that one can estimate $\mathbf{k}^2=\mathbf{l}^2\approx 6m_NT$. Then, we find for the momentum dependent terms of (A.1)

$$\left(\frac{\mathbf{k}^2}{\mathbf{k}^2+m_\pi^2}\right)^2 \approx \left(\frac{\mathbf{l}^2}{\mathbf{l}^2+m_\pi^2}\right)^2 \approx \left(\frac{1}{1+\frac{m_\pi^2}{6m_NT}}\right)^2 \equiv \xi(T) \tag{A.3}$$

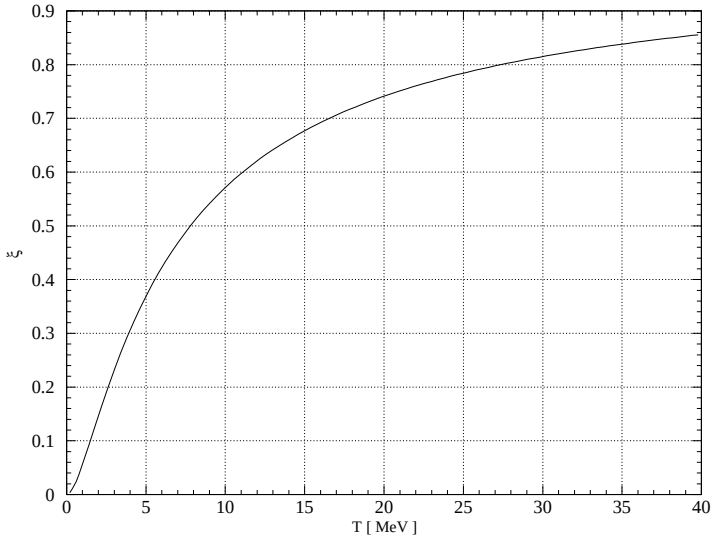

Figure A.1: The factor $\xi(T)$ as defined in (A.3).

and

$$\frac{\mathbf{k}^2\,\mathbf{l}^2 - 3(\mathbf{k}\cdot\mathbf{l})^2}{(\mathbf{k}^2+m_\pi^2)(\mathbf{l}^2+m_\pi^2)} \approx \xi(T) - \beta\,\xi(T)\ . \tag{A.4}$$

Altogether, we finally obtain for the squared matrix element

$$\sum_s |\mathcal{M}|^2 \;=\; \frac{256\pi^2}{3}\frac{g_{aN}^2\alpha_\pi^2}{m_N^2}\xi(T)\ (3-\beta) \tag{A.5}$$

$$\equiv\; \xi(T)\ \sum_s |\mathcal{M}|^2\Big|_{m_\pi=0}\ , \tag{A.6}$$

i.e. all effects attributed to a non vanishing pion mass m_π are combined in the overall factor $\xi(T)$. In Fig. A.1, the function $\xi(T)$ is plotted for temperatures between 0 and 40 MeV. This simple estimation of pion mass effects is in good agreement with the exact calculation of Raffelt and Seckel [34]. However, our approximation underestimates the reduction of axion emission rates due to the pions mass: At temperatures around 10 MeV the exact result predicts a reduction of about 50%, in contrast to our estimation, which yields 57%.

Appendix B

Nucleons and Electrons in Neutron Stars

We consider a nuclear medium which is made up of protons, neutrons, electrons and neutrinos. We assume that all particle species are in chemical equilibrium with each other as result of the reaction $e + p \leftrightarrow n + \nu_e$. In addition, neutrinos are allowed to stream freely away, i.e. their chemical potential vanishes $\mu_\nu = 0$. The phase-space occupation function of each species $i = p, n, e, \nu_e$ is given by the Fermi-Dirac distribution

$$f(\mathbf{p}_i) = \frac{1}{\exp[(E_i(\mathbf{p}_i) - \mu_i)/T] + 1} \ , \tag{B.1}$$

with the energy $E_i(\mathbf{p}_i)^2 = m_i^2 + \mathbf{p}_i^2$ and the chemical potential μ_i. The value of μ_i at $T = 0$ defines the Fermi energy $E_{F,i}^2 = m_i^2 + p_{F,i}^2$ in terms of the Fermi momentum $p_{F,i}$, which is related to the particle's number density by $n_i = g\, p_{F,i}^3/6\pi^2$ with $g = 1$ for neutrinos and $g = 2$ for nucleons and electrons. For a nonrelativistic particle species (neutrons and protons in neutron stars), it is appropriate to use the nonrelativistic Energie $E_i^{\rm kin} = E_i(\mathbf{p}_i) - m_i \approx \mathbf{p}_i^2/2\, m_i,\ i = n, p$ and the nonrelativistic chemical potential $\hat{\mu}_i \equiv \mu_i - m_i$.

It is useful to introduce the neutron and proton number fractions Y_n and Y_p, respectively. They are defined as

$$Y_n = n_n/n_B \quad \text{and} \quad Y_p = n_p/n_B \ , \tag{B.2}$$

where $n_B \equiv (N_p + N_n)/V$ is the total baryon number density. Consequently, $Y_p + Y_n = 1$. Furthermore, the electron fraction $Y_e = n_e/n_B$ describes the number of electrons per baryon. As a result of charge neutrality, the electron fraction is equal to the proton fraction, $Y_e = Y_p$.

The number fractions Y_p and Y_n can be determined easily for neutron stars if one works on the assumption that the star is transparent to neutrinos, i.e. $\mu_{\nu_e} = 0$. This is justified since we cosider quite cold neutron stars. One then obtains the proton fraction in the case of a degenerate medium [48]

$$Y_p = \frac{n_p/n_n}{n_p/n_n + 1} \tag{B.3}$$

with

$$\frac{n_p}{n_n} \approx \frac{1}{8}\left(\frac{1 + 4Q/m_n\, x_n^2 + 4(Q^2 - m_e^2)/m_n^2\, x_n^4}{1 + 1/x_n^2}\right)^{3/2}, \tag{B.4}$$

where $Q = m_n - m_p = 1.29$ MeV, $x_n = p_{F,n}/m_n$, and $p_{F,n}$ is the Fermi momentum of the neutron. From that, the neutron and electron number fractions follow immediately through $Y_n = 1 - Y_p$ and $Y_e = Y_p$.

We are concerned with neutron stars which have characteristic densities of $\rho_B \approx 2\rho_{\text{nuc}} \approx 5.6 \times 10^{14}$ g cm^{-3} and core temperatures less than 100 keV. Then, one explicitly finds $Y_p \approx 0.009$, i.e. nuclear matter in neutron stars is approximately made up of 99% neutrons and 1% protons. However, it should be stressed that these values depeds strongly on the underlying equation of state. Moreover, a neutron star is not just a homogeneous ball but consists diverent layers like the outer crust, inner crust, outer core, and inner core. Another problem is that in a dense medium nucleon interactions become important so that the ideal gas is no longer a good approximation of the equation of state. As a consequence, the nucleon effective mass m_N^* is less than its vacuum value, and its thermal excitations depend on a uncertain dispersion relation. Summing up, we conclude that the proton fraction in neutron star is a few percent of the neutron number.

Bibliography

[1] http://www-spires.slac.stanford.edu/spires/hep/

[2] I. Ogawa, S. Matsuki, K. Yamamoto, Phys. Rev. D **53**, 1740 (1996);
K. Yamamoto, S. Matsuki, hep-ph/9811487

[3] C. Hagmann et al. Phys. Rev. Lett. **80**, 2043 (1998)

[4] T. Moroi, H. Murayama, Phys.Lett. B **440**, 69 (1998)

[5] G. Raffelt, hep-ph/9903472 (1999)

[6] D.B. Kaplan, Nucl. Phys. B **260**, 215 (1985)

[7] M. Ruffert, H.-T. Janka, astro-ph/9809280 (1998)

[8] H. Umeda, astro-ph/9806337 (1998)

[9] R. D. Peccei, H. R. Quinn, Phys. Rev. Lett. **38**, 1440 (1977);
R. D. Peccei, H. R. Quinn, Phys. Rev. D **16**, 1791 (1977)

[10] M.E. Peskin, D.V.Schroeder, *An Introduction to Quantum Field Theory* (Addison-Wesley Publishing Company, 1997)

[11] W.A. Bardeen, S.H.H. Tye, Phys. Lett. B **74**, 580 (1978)

[12] B. Renner, *Current Algebras And Their Applications* (Pergamon Press, 1968)

[13] H. Leutwyler, Phys. Lett. B **378**, 313 (1996)

[14] C. Caso et al. Eur.Phys.J. C 3, 1 (1998)

[15] M. Srednicki, Nucl. Phys. B **260**, 689 (1985)

[16] W. Keil et al. Phys. Rev. D **56**, 2419 (1997)

[17] G. Raffelt, *Stars as Laboratories for Fundamental Physics* (University of ChicagoPress, 1996)

[18] M.S. Turner, Phys. Rev. Lett. **60**, 1797 (1988)

[19] A. Burrows, M.T. Ressel, M.S. Turner, Phys. Rev. D **42**, 3297 (1990)

[20] H.T. Janka, W. Keil, G. Raffelt, D. Seckel, Phys. Rev. Lett. **76**, 2621 (1996)

[21] J. Engel, D. Seckel, A.C. Hayes, Phys. Rev. Lett. **65**, 960 (1990)

[22] E.W. Kolb, M.S. Turner, Phys. Rev. Lett. **62**, 509 (1989)

[23] J.M Overduin, P.S. Wesson, Ap. J. **414**, 449 (1993)

[24] M.T. Ressell, Phys. Rev. D **44**, 3001 (1991)

[25] K.A. Olive, G. Steigman, T.P. Walker, astro-ph/9905320

[26] P.J. Kernan, S. Sarkar, Phys. Rev. D **54**, 3681 (1996)

[27] S. Sarkar, Rept. Prog. Phys. **59**, 1493 (1996)

[28] M. Turner, Phys. Rev. Lett. **59**, 2489 (1987)

[29] E.W. Kolb, M.S. Turner, *The early universe* (Addison-Wesley Publishing Company, 1994)

[30] S. Chang, K. Choi, Phys. Lett. B **316**, 51 (1993)

[31] B. Novosyadlyj, astro-ph/9903357 (1999)

[32] R. Valdarnini, T. Kahniashvili, B. Novosyadlyj, astro-ph/9804057 (1998)

[33] R.P. Brinkmann, M.S. Turner, Phys. Rev. D **38**, 2338 (1988)

[34] G. Raffelt, D. Seckel, Phys. Rev. D **52**, 1780 (1995)

[35] M.S. Briggs et al. astro-ph/9509078 (1995)

[36] E. Costa et al. Nature **387**, 783 (1997)

[37] J. van Paradijs et al. Nature **386**, 686 (1997)

[38] D. Frail et al. Nature **395**, 663 (1998)

[39] M.H. Ruffert, H.T. Janka, G. Schafer, A&A **311**, 532 (1996);
M.H. Ruffert, H.T. Janka, K. Takahashi, G. Schafer, A&A **319**, 122 (1997);
M.H. Ruffert, H.T. Janka, astro-ph/9804132 (1998)

[40] S. Moriyama, Phys. Rev. Lett. **75**, 3222 (1995)

[41] M. Krčmar et al. Phys. Lett. B **442**, 38 (1998)

[42] E.H. Gudmundsson, C.J. Pethick, R.I. Epstein, Ap. J. **272**, 286, (1983)

[43] H. Ögelman, J. P. Finley, ApJ **413**, L31 (1993)

[44] J. P. Halpern, F. Y.-H. Wang, ApJ **477**, 905 (1997)

[45] A. Possenti, S. Mereghetti, M. Colpi, A&A **313**, 565 (1996)

[46] F. A. Rasio, S. L. Shapiro, Class.Quant.Grav. **16**, R1 (1999)

[47] C. Schaab et al. ,astro-ph/9904127 (1999)

[48] S. L. Shapiro, S. A. Saul, *Black Holes, White Dwarfs, and Neutron Stars* (John Wiley & Sons, Inc, 1983)

[49] S. Tsuruta, Phys. Repts. **292**, 1 (1998)

[50] D. G. Yakovlev, K. P. Levenfish, Yu. A. Shibanov, astro-ph/9906456 (1999)